© 2016. Published by The Company of Biologists Ltd | Development (2016) 143, 1328-1339 doi:10.1242/dev.132654

RESEARCH ARTICLE

Clarification of mural cell coverage of vascular endothelial cells by live imaging of zebrafish

Koji Ando[1], Shigetomo Fukuhara[1,*], Nanae Izumi[2], Hiroyuki Nakajima[1], Hajime Fukui[1], Robert N. Kelsh[3] and Naoki Mochizuki[1,4,*]

ABSTRACT

Mural cells (MCs) consisting of vascular smooth muscle cells and pericytes cover the endothelial cells (ECs) to regulate vascular stability and homeostasis. Here, we clarified the mechanism by which MCs develop and cover ECs by generating transgenic zebrafish lines that allow live imaging of MCs and by lineage tracing *in vivo*. To cover cranial vessels, MCs derived from either neural crest cells or mesoderm emerged around the preformed EC tubes, proliferated and migrated along EC tubes. During their migration, the MCs moved forward by extending their processes along the inter-EC junctions, suggesting a role for inter-EC junctions as a scaffold for MC migration. In the trunk vasculature, MCs derived from mesoderm covered the ventral side of the dorsal aorta (DA), but not the posterior cardinal vein. Furthermore, the MCs migrating from the DA or emerging around intersegmental vessels (ISVs) preferentially covered arterial ISVs rather than venous ISVs, indicating that MCs mostly cover arteries during vascular development. Thus, live imaging and lineage tracing enabled us to clarify precisely how MCs cover the EC tubes and to identify the origins of MCs.

KEY WORDS: Mural cells, Pericytes, Vascular smooth muscle cells, Zebrafish, Pdgfrb

INTRODUCTION

The vasculature consists of two principle cell types: endothelial cells (ECs) and mural cells (MCs). ECs line the inner surface of the blood vessels, whereas the MCs cover the abluminal surface of the ECs. MCs are further classified into two types: vascular smooth muscle cells (VSMCs) and pericytes (Gaengel et al., 2009). The former consist of multi-layered cells and ensheath ECs, whereas the latter are solitary cells associated with small diameter blood vessels, such as arterioles, venules and capillaries. MCs play an essential role in vascular stability and homeostasis (Armulik et al., 2011). Therefore, loss or detachment of MCs leads to various vascular diseases (French et al., 2014; Garg et al., 2014; Joutel et al., 1996).

MCs originate from distinct developmental precursors such as mesoderm-derived mesenchymal cells and neural crest cells (Majesky, 2007; Wasteson et al., 2008; Winkler et al., 2011). These precursors are thought to be recruited to the vessel wall and to differentiate into MCs, which subsequently proliferate and migrate to cover entire vessels (Armulik et al., 2011; Hellstrom et al., 1999). However, when and how the progenitor cells differentiate into MCs and cover the blood vessels during vascular development remains largely unknown, because no clear methods for analyzing MCs in living animals have been developed. To date, although zebrafish transgenic (Tg) lines, such as *Tg(sm22a-b:GFP)* and *Tg(acta2:EGFP)*, have been developed to visualize MCs *in vivo* (Seiler et al., 2010; Whitesell et al., 2014), only limited parts of vasculature were covered by perivascular enhanced green fluorescent protein (EGFP)-expressing cells in these Tg zebrafish lines. Thus, these fish lines may not faithfully report all MCs *in vivo*.

The platelet-derived growth factor (PDGF)-B/PDGF receptor β (PDGFRβ) signaling pathway plays a crucial role in the regulation of MC coverage of blood vessels (Hellstrom et al., 1999; Olson and Soriano, 2011; Wang et al., 2014). PDGF-B secreted from ECs binds to PDGFRβ receptors expressed on the MCs, thereby promoting recruitment of MCs and their subsequent proliferation and migration. Recently, Wang et al. successfully visualized pericytes covering cerebral vessels in the zebrafish brain by performing fluorescence *in situ* hybridization (ISH) for *pdgfrb* (Wang et al., 2014). However, this method does not allow the analysis of MC dynamics *in vivo*.

Here, we have succeeded in visualizing the MCs in living zebrafish by developing Tg lines in which EGFP, mCherry or the Gal4FF driver, an engineered transcriptional activator consisting of the DNA-binding domain from Gal4 fused to two transcription activation modules from VP16 (Asakawa et al., 2008), was expressed under the control of *pdgfrb* promoter. Exploiting these Tg lines, we demonstrated how MCs develop and cover ECs in the cranial and trunk vessels and identified the origins of MCs covering the cranial and trunk vasculature.

RESULTS

Development of Tg zebrafish lines for live imaging of MCs

The *Pdgfrb* promoter is activated in MCs of mice (Foo et al., 2006). To visualize MCs using living animals, we developed *TgBAC(pdgfrb:EGFP)*, *TgBAC(pdgfrb:mCherry)* and *TgBAC(pdgfrb:Gal4FF);Tg(UAS:GFP)* zebrafish lines, in which EGFP, mCherry or the Gal4FF driver was expressed under control of *pdgfrb* promoter, respectively (Fig. 1A). To simultaneously visualize ECs and MCs, the first and the third lines were crossed with *Tg(fli1a:myryistoylation-signal tagged (Myr)-mCherry)* fish. The second line was crossed with *Tg(fli1a:Myr-EGFP)*. The expression pattern of fluorescent proteins in these reporter lines was similar to the previously reported expression pattern of *pdgfrb* mRNA (Wang et al., 2014; French et al., 2014; Wiens et al., 2010). In the *TgBAC(pdgfrb:EGFP)* embryos, EGFP started to be expressed around the 8-somite stage in the cranial neural crests in which *pdgfrb* mRNA is expressed (French et al., 2014) (Fig. S1A,B; Movies 1 and 2). EGFP expression was induced in the base of the brain from 17 h post-

[1]Department of Cell Biology, National Cerebral and Cardiovascular Center Research Institute, 5-7-1 Fujishirodai, Suita, Osaka 565-8565, Japan. [2]Frontier Research Laboratories, R&D Division, Daiichi Sankyo Co., Ltd., 1-2-58, Hiromachi, Shinagawa-ku, Tokyo 140-8710, Japan. [3]Centre for Regenerative Medicine, Developmental Biology Programme, Department of Biology and Biochemistry, University of Bath, Bath BA2 7AY, UK. [4]AMED-CREST, Department of Cell Biology, National Cerebral and Cardiovascular Center Research Institute, 5-7-1, Suita, Osaka 565-8565, Japan.

*Authors for correspondence (fuku@ncvc.go.jp; nmochizu@ncvc.go.jp)

Received 3 November 2015; Accepted 24 February 2016

Development (2016) 143, 1328-1339 doi:10.1242/dev.132654

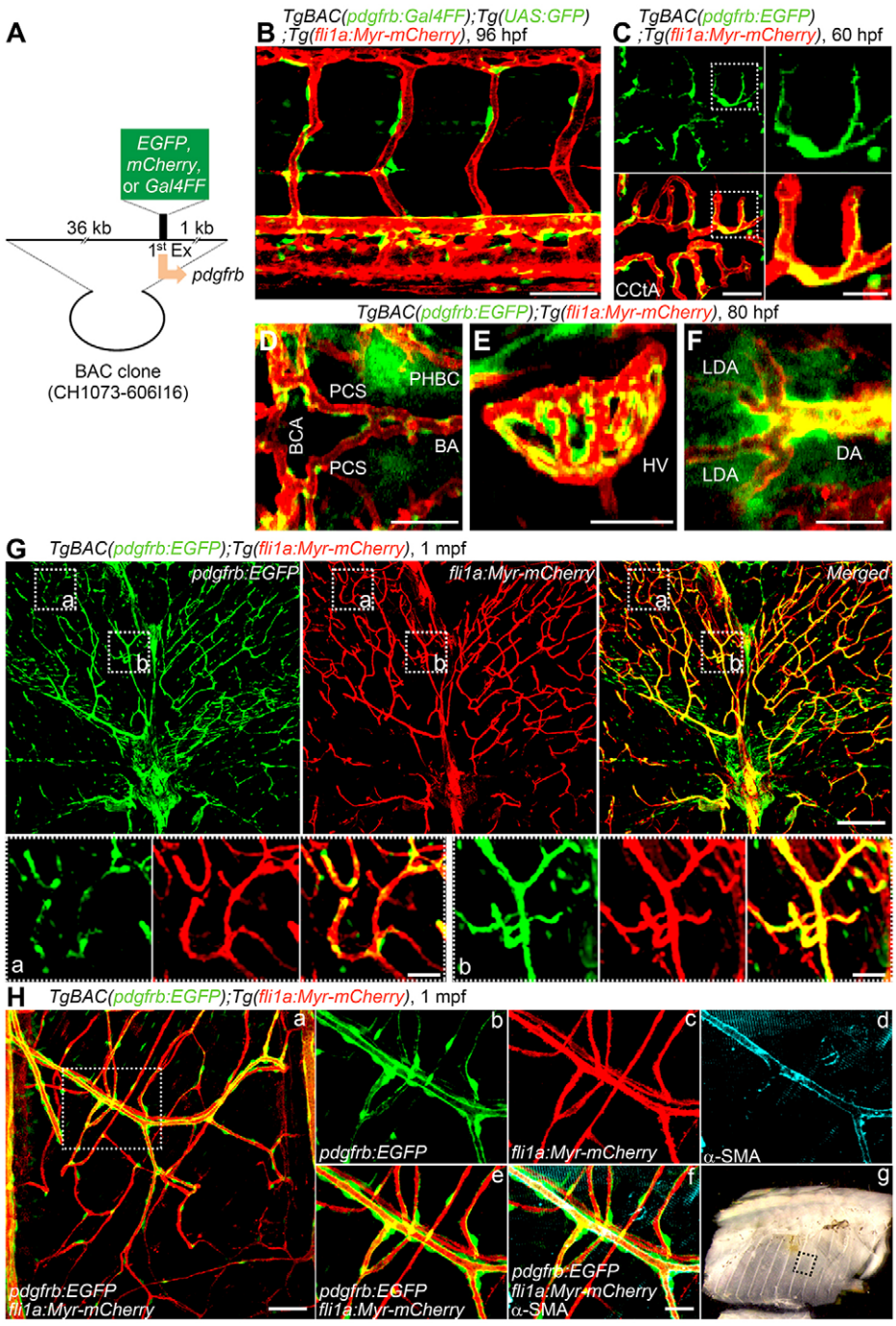

Fig. 1. Generation of Tg zebrafish lines for live imaging of MCs. (A) A schematic structure of the BAC clone (CH1073-606I16) used to generate Tg zebrafish lines for live imaging of MCs. cDNA encoding either EGFP, mCherry or Gal4FF was inserted at the start codon of *pdgfrb* gene. (B) Confocal stack fluorescence image of trunk vasculature in a 96 hpf *TgBAC(pdgfrb:Gal4FF);Tg(UAS:GFP);Tg(fli1a:Myr-mCherry)* larva. Lateral view, anterior to the left. Merged image of *pdgfrb:Gal4FF;UAS:GFP* (green) and *fli1a:Myr-mCherry* (red). (C-F) Confocal images of hindbrain vasculature (C,D), hyaloid vessels (E) and anterior region of dorsal aorta (F) in the *TgBAC(pdgfrb:EGFP);Tg(fli1a:Myr-mCherry)* larvae at 60 hpf (C) and 80 hpf (D-F). Dorsal view, anterior to the left. Merged images of *pdgfrb:EGFP* (green) and *fli1a:Myr-mCherry* (red). In C, the boxed areas are enlarged to the right. (G) Confocal images of trunk vasculature in a 1 mpf *TgBAC(pdgfrb:EGFP);Tg(fli1a:Myr-mCherry)* juvenile. Cross-sectional views (200 µm thick) through the caudal region as depicted in Fig. S1H are shown. Upper left, *pdgfrb:EGFP* (green); upper center, *fli1a:Myr-mCherry* (red); upper right, merged image. The boxed areas labeled a and b are enlarged below. (H) Confocal images of blood vessels in the intercostal muscle of a 1 mpf *TgBAC(pdgfrb:EGFP);Tg(fli1a:Myr-mCherry)* juvenile. Pleural tissue as indicated by the box shown in g was cut out and immunostained with anti-α-SMA antibody to visualize VSMCs. The merged image of *pdgfrb:EGFP* (green) and *fli1a:Myr-mCherry* (red) is shown on the left (a). The boxed area in a is enlarged to the right: *pdgfrb:EGFP* (b), *fli1a:Myr-mCherry* (c), α-SMA (d), merge of *pdgfrb:EGFP* (green) and *fli1a:Myr-mCherry* (red) (e) and merge of *pdgfrb:EGFP* (green), *fli1a:Myr-mCherry* (red) and α-SMA (blue) (f). (g) Brightfield image of the thorax showing the region where the image shown in a was taken. BA, basilar artery; BCA, basal communicating artery; CCtA, cerebellar central artery; DA, dorsal aorta; LDA, lateral DA; HV, hyaloid vessel; PCS, posterior communicating segment; PHBC, primordial hindbrain channel. Scale bars: 20 µm (enlarged images in C and H; D-F); 50 µm (B,C); 100 µm (G,H).

fertilization (hpf) (Fig. S1A,B; Movies 1 and 2). In the trunk of the *TgBAC(pdgfrb:EGFP)* and *TgBAC(pdgfrb:mCherry)* embryos, fluorescence signal was observed in the floor plate and hypochord at 24 hpf (Fig. S1C). At late stages, the dorsal aorta (DA), intersegmental vessels (ISVs) and dorsal longitudinal anastomotic vessels were surrounded by EGFP-positive cells in the trunk region of *TgBAC(pdgfrb:Gal4FF);Tg(UAS:GFP)* larvae (Fig. 1B). In the head region of *TgBAC(pdgfrb:EGFP)* larvae, EGFP-positive cells covered the vessels, such as the central artery (CtA), basal communicating artery (BCA), posterior communicating segment (PCS), basilar artery (BA), primordial hindbrain channel (PHBC) and hyaloid vessels (HVs) (Fig. 1C-E). In addition, EGFP-positive cells were accumulated in the anterior region of the DA, including the lateral DA where Transgelin-positive MCs also exist (Fig. 1F) (Santoro et al., 2009). Similarly, perivascular cells in the cranial and trunk vessels were visualized by mCherry in the *TgBAC(pdgfrb:mCherry);Tg(fli1a:Myr-EGFP)* larvae (Fig. S1D,E). These results indicate that fluorescent proteins successfully label MCs in our reporter lines. Indeed, RT-PCR analyses revealed that EGFP-positive cells isolated from *TgBAC(pdgfrb:EGFP);Tg(fli1a:Myr-mCherry)* larvae expressed not only *pdgfrb* but also other MC marker genes, such as *chondroitin sulfate proteoglycan 4* (*cspg4*) and *actin, alpha 2, smooth muscle, aorta* (*acta2*) (Fig. S1F).

We also visualized VSMCs by generating the *TgBAC(tagln:EGFP)* zebrafish line, in which EGFP is expressed under the control of smooth muscle-specific *transgelin* promoter (Robin et al., 2013). Larvae of this Tg fish exhibited EGFP signal in the floor plate, swim bladder, gut and rostral notochord (Fig. S1G). In addition, EGFP-

Development (2016) 143, 1328-1339 doi:10.1242/dev.132654

positive cells were detected in the ventral part of the DA, but not in the cranial vessels (data not shown), as previously observed in the *Tg(sm22a-b:GFP)* zebrafish line (Seiler et al., 2010). These findings indicate that the *TgBAC(tagln:EGFP)* line labels VSMCs *in vivo*.

Live imaging of blood vessel MCs in juvenile zebrafish

Next, we investigated whether MCs can be labeled by EGFP in the juvenile *TgBAC(pdgfrb:EGFP)* zebrafish. At 1 month post-fertilization (mpf), most blood vessels in the trunk were covered by EGFP-positive cells (Fig. 1G; Fig. S1H). Blood vessels with a diameter >5-10 µm were continuously ensheathed by EGFP-positive cells and were also stained with antibody for the VSMC marker α-SMA (Acta2), indicating that EGFP-positive cells were VSMCs in the *TgBAC(pdgfrb:EGFP)* zebrafish (Fig. 1G,H). Consistently, these thick vessels were also EGFP-positive in the *TgBAC(tagln:EGFP)* zebrafish line (Fig. S1I). By contrast, the capillaries with a diameter <5 µm were irregularly and discontinuously covered by EGFP-positive cells in the *TgBAC (pdgfrb:EGFP)* fish, but not in the *TgBAC(tagln:EGFP)* line (Fig. 1G,H; Fig. S1I), suggesting that EGFP-positive cells covering the capillaries are pericytes. Thus, our *TgBAC(pdgfrb:EGFP)* line precisely monitors pericytes and VSMCs.

Live imaging of MC coverage of cranial vessels

To investigate how cranial vessels become covered by MCs, we time-lapse imaged the *TgBAC(pdgfrb:EGFP);Tg(fli1a:Myr-mCherry)* embryos, focusing on the MCs covering the CtA, which consists of cerebellar CtA (CCtA), anterior mesencephalic CtA (AMCtA), middle mesencephalic CtA (MMCtA) and posterior mesencephalic CtA (PMCtA). The CCtA are formed by ECs sprouting from the PHBC. The sprouting CCtA ECs from the PHBC first migrate dorsally to penetrate the hindbrain parenchyma, then turn ventrally and connect to the BA at 40-48 hpf (Fujita et al., 2011). During CCtA formation, weakly EGFP-positive cells existed in the cerebral base at the level of the BA (Fig. 2A). The location of the EGFP-positive cells implied that they might be anterior endodermal cells. However, they were not identical to *sox17* promoter-active endodermal cells (Fig. S2A). Among the weakly EGFP-positive cells, cells located in the vicinity of the BA started to emit strong green fluorescence and then made tight contact with the BA (Fig. 2A). At ∼60 hpf, strongly EGFP-positive cells covering the BA started to migrate along the CCtA and frequently proliferated to cover the ECs throughout the CCtA (Fig. 2B,C; Movies 3-5). These results indicate that the CCtA is covered by MCs that originally emerge around the BA (Fig. 2D).

MC differentiation around the BA implies an instructive role for the BA in MC development. Consistently, *kdr*/*kdrl*-double morphants, which failed to develop the BA, exhibited a lack of strongly EGFP-positive cells in the midline of the hindbrain (Fig. S2B). Although EC function is influenced by blood flow, loss of blood flow did not affect MC emergence around the BA but did prevent their subsequent recruitment into the CtA (Fig. S2C). These results suggest that ECs regulate MC development independently of blood flow, whereas MC recruitment might be promoted by a flow-dependent EC-derived signal.

We also investigated how MCs are recruited to the AMCtA, MMCtA and PMCtA. These CtA vessels extend from the vessels located in the cerebral base, such as the BCA, PCS and choroidal vascular plexus (CVP), and subsequently penetrate into the brain parenchyma (Isogai et al., 2003). Weakly EGFP-positive cells located in close proximity to the BCA, PCS and CVP started to emit strong green fluorescence and were recruited to the AMCtA, MMCtA and PMCtA (Fig. S2D; Movies 4 and 5). By 120 hpf, most of the CtA vessels became surrounded by strongly EGFP-positive cells that no longer proliferated and migrated (data not shown). Collectively, these results suggest that the CtA vessels are covered by MCs that originally differentiated around the vessels located in the cerebral base.

Pdgfrβ signaling is involved in recruitment and proliferation of MCs during embryogenesis (Hellstrom et al., 1999; Olson and Soriano, 2011; Wang et al., 2014). Thus, we analyzed *pdgfrb*$^{sa16389/sa16389}$ mutant larvae, which lack functional Pdgfrβ to clarify the role of Pdgfrβ in MC coverage of cranial vessels (Fig. 2E; Fig. S2E). The *pdgfrb* mutant larvae developed cranial vessels normally and exhibited MC coverage of PCS, BCA and BA located in the cerebral base. However, they lost MC coverage of the CtA. Similarly, the number of MCs covering the CtA was reduced by treatment with AG1296, a Pdgfrβ inhibitor (Fig. S2F). These results suggest that Pdgfrβ signaling is dispensable for MC differentiation around the vessels located in the cerebral base, but indispensable for their subsequent recruitment into the CtA.

MC migration along inter-EC junctions

We further investigated how MCs migrate along the EC tube to cover the CtA by utilizing the *Tg(fli1a:pecam1-EGFP)* line, in which inter-EC junctions are visualized by Pecam1-EGFP. Time-lapse imaging revealed that MCs preferentially extended their processes along inter-EC junctions during their migration along the CtA (Fig. 3A; Movie 6). The tip of the extending process attached to the inter-EC junction in ∼70% of the cases (Fig. S3A). In addition, ∼60% of the total length of the processes was aligned along the inter-ECs junctions (Fig. 3B; Fig. S3B; Movie 7). Importantly, some parts of the processes spread widely on the inter-EC junctions as if the junctions became scaffold structures for MC migration (Fig. 3C). Consistently, of the 30 MCs migrating along the CtA that we analyzed, 90% moved forward by sequentially relocating their cell bodies to the scaffold structures formed within the preceding processes (Fig. 3C; Movie 8). When the MCs migrated across the unicellular tube, they extended their processes around the EC tube even in the absence of contact with the inter-EC junctions (Fig. S3C; Movie 9). However, once the tip of the processes reached the inter-EC junctions, the MCs further extended their processes along the junctions and established the scaffold structures within these processes (Fig. S3C; Movie 9). These results suggest that during MC coverage of CtA, MCs extend their processes along inter-EC junctions and establish the scaffold structures required within the processes to move forward (Fig. 3D).

Live imaging of MC coverage of axial vessels in the trunk

Next, we analyzed MC coverage of trunk axial vessels by time-lapse imaging of the *TgBAC(pdgfrb:EGFP);Tg(fli1a:Myr-mCherry)* fish. EGFP-positive cells started to emerge in the ventral part of the DA at 36 hpf, whereas the posterior cardinal vein (PCV) was not covered by EGFP-positive cells until at least 7 dpf (Fig. 4A; data not shown). Unfortunately, we could not analyze MC emergence in the dorsal side of the DA because of EGFP expression in the hypochord, which is located just along the dorsal side of the DA (Fig. 4A; Fig. S1C). However, we confirmed that EGFP-positive cells in the ventral part of the DA did not originate from the hypochord. EGFP-positive cells emerged at the ventral side of the DA, gradually emitted strong fluorescence and underwent cell division frequently (Fig. 4A; Movie 10). These EGFP-positive cells dorsally extended multiple processes, irrespective of the presence of

Development (2016) 143, 1328-1339 doi:10.1242/dev.132654

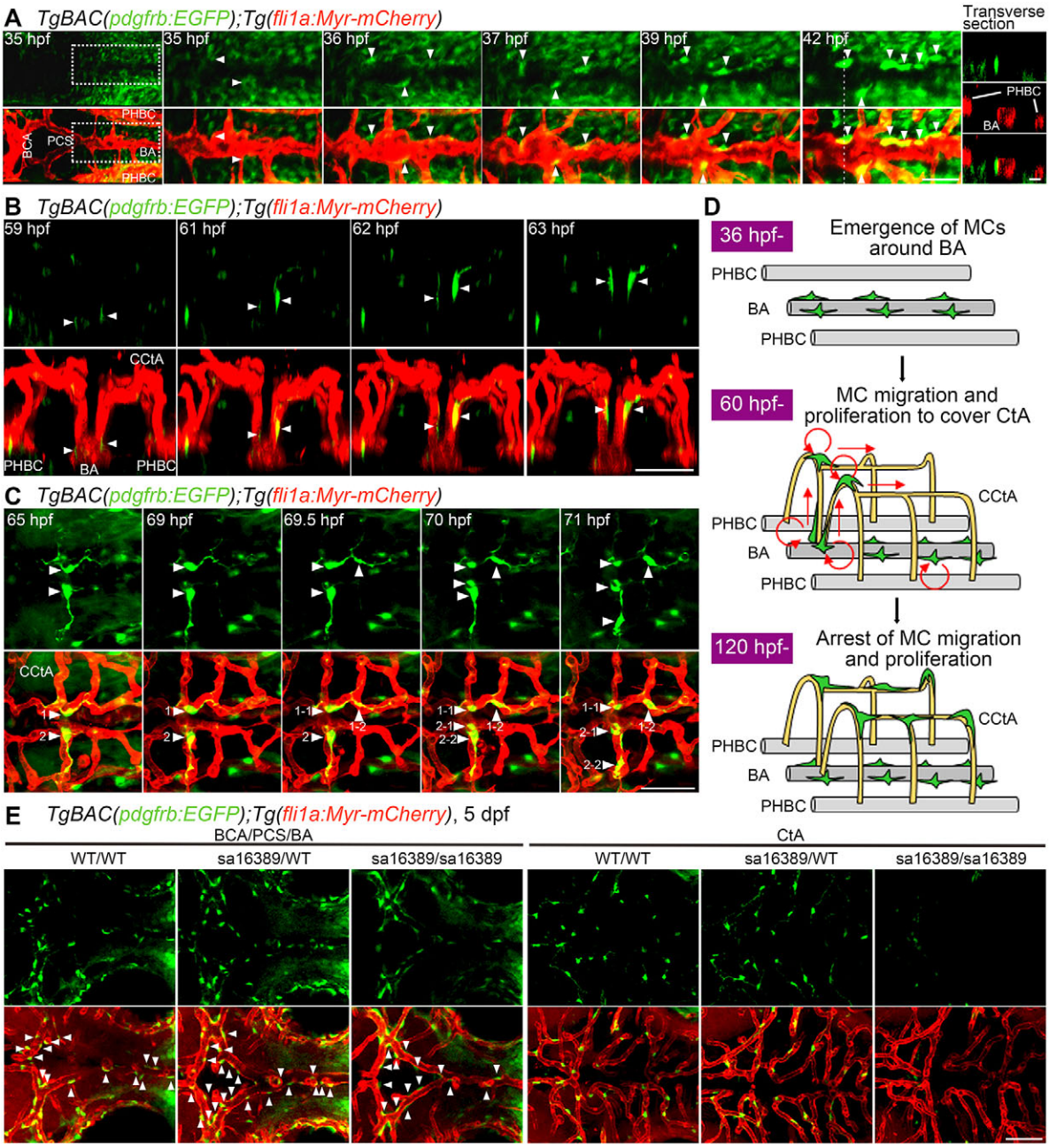

Fig. 2. Live imaging of MC coverage in cranial vessels. (A-C) Time-lapse confocal images of the hindbrain vasculature in *TgBAC(pdgfrb:EGFP);Tg(fli1a:Myr-mCherry)* larvae at 35-42 hfp (A), 59-63 hpf (B) and 65-71 hpf (C). Upper, *pdgfrb:EGFP*; lower, merged images of *pdgfrb:EGFP* (green) and *fli1a:Myr-mCherry* (red). (A) Dorsal view, anterior to the left. The central panels are enlarged and subsequent time-lapse images of the boxed areas in the leftmost column. The transverse sectional views of the areas indicated by dashed lines on the 42 hpf image are shown in the rightmost column. Top, *pdgfrb:EGFP* (green); middle (rightmost column only), *fli1a:Myr-mCherry* (red); bottom, merged image. Note that the cells located in the vicinity of the BA (arrowheads) gradually emitted strong EGFP signal and tightly contacted ECs. (B) 3D-rendered confocal images of EGFP-positive cells (green) migrating along the CCtAs. Lateral view, dorsal to the top and anterior to the front. Note that EGFP-positive cells located around the BA (arrowheads) dorsally migrated along the CCtAs. (C) Dorsal view, anterior to the left. Arrowheads with numbers indicate individual EGFP-positive cells spreading on the CCtAs. Note that EGFP-positive cells spreading on the CCtA (1 and 2) divided into two daughter cells (1-1/1-2 and 2-1/2-2). (D) Schematic of how CCtAs become covered by MCs. MCs develop around the BA and migrate towards the CCtAs. During their migration, the MCs actively proliferate to cover the CCtAs. (E) Confocal images of hindbrain vasculature of *pdgfrb* wild-type (WT/WT), heterozygous (sa16389/WT) and homozygous (sa16389/sa16389) larvae in the *TgBAC(pdgfrb:EGFP);Tg(fli1a:Myr-mCherry)* background at 5 dpf. Dorsal view, anterior to the left. The vessels in the cerebral base, such as BCA, PCA and BA (BCA/PCS/BA), and the CtA, are shown in the left and right columns, respectively. Upper, *pdgfrb:EGFP*; lower, merged images of *pdgfrb:EGFP* (green) and *fli1a:Myr-mCherry* (red). Arrowheads indicate MCs emerged around the BCA, PCS and BA. Scale bars: 20 µm (transverse sectional image in A); 50 µm (A,B,C,E).

inter-EC junctions, to ensheath the DA wall (Fig. S4A). Proliferation of MCs at the ventral part of the DA was confirmed by utilizing the Fucci (fluorescent ubiquitination-based cell cycle indicator) system (Sakaue-Sawano et al., 2008). We generated a Tg zebrafish line in which NLS-mCherry and mVenus-geminin, a Fucci biosensor for visualizing cells in S/G2/M phases, were simultaneously expressed in *pdgfrb* promoter-activated cells. The mCherry/mVenus double-positive cells at the ventral side of the DA

Development (2016) 143, 1328-1339 doi:10.1242/dev.132654

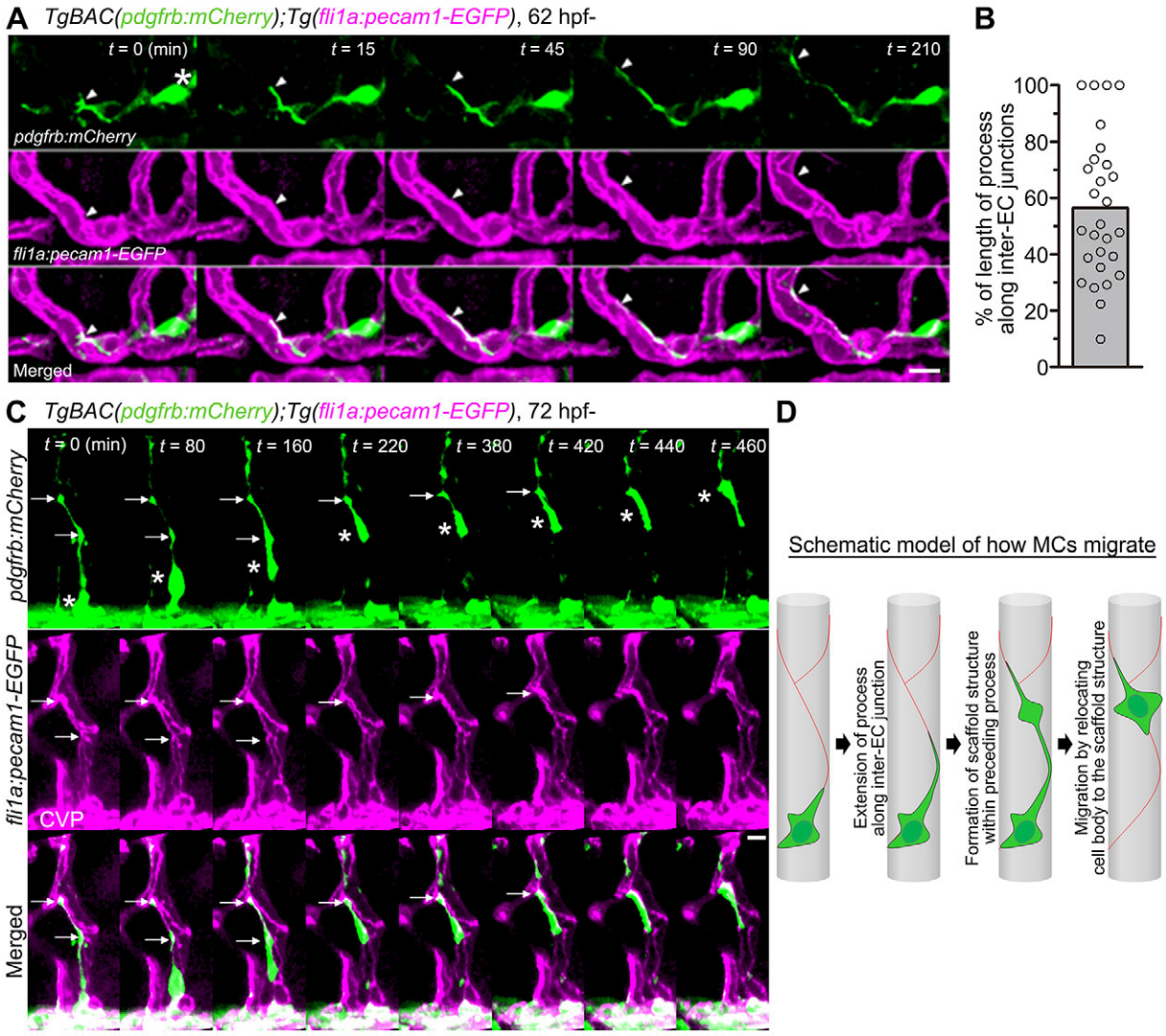

Fig. 3. Migration of MCs along inter-EC junctions. (A) Time-lapse confocal images of an MC migrating along the CtA in the hindbrain of a *TgBAC(pdgfrb:mCherry);Tg(fli1a:pecam1-EGFP)* larva. 3D-rendered confocal images at 62 hpf (leftmost column) and their subsequent time-lapse images with the elapsed time (min) at the top right. Top, *pdgfrb:mCherry* (green); middle, *fli1a:pecam1-EGFP* (magenta); bottom, merged images. Arrowheads and asterisk indicate the tip of the MC process and the cell body, respectively. Note that the MC extended a process along the Pecam1-EGFP-labeled inter-EC junctions. (B) Alignment of MC processes along inter-EC junctions, as observed in A, expressed as a percentage of the total length (n=28). Bar and circles indicate the average and the values of individual processes, respectively. (C) Time-lapse confocal images of an MC migrating along the CtA, as in A. 3D-rendered confocal images at 72 hpf (leftmost column) and their subsequent time-lapse images with the elapsed time (min) at the top right. Note that the MC moved forward by sequentially relocating its cell body (asterisks) to the punctate structures formed within the preceding processes (arrows). CVP, choroidal vascular plexus. (D) Schematic of how MCs migrate along the EC tube to cover the CtA. Red lines indicate the inter-EC junctions, green cells represent MCs. Scale bars: 10 µm (A,C).

apparently divided into two daughter cells, which subsequently lost mVenus fluorescence, but retained mCherry fluorescence, although these fluorescent proteins tended to be expressed in a mosaic fashion (Fig. 4B). These findings indicate that MCs cover the DA by differentiation at the ventral part of the DA and by their subsequent proliferation.

We analyzed MC coverage of the DA by utilizing the *TgBAC (tagln:EGFP)* zebrafish line to visualize VSMCs. In the *TgBAC (pdgfrb:Gal4FF);Tg(UAS:RFP);TgBAC(tagln:EGFP)* larvae at 7 dpf, EGFP/RFP double-positive cells were observed in the ventral part of the DA (Fig. S4B,C), indicating that the MCs emerging on the ventral side of the DA were *pdgfrb*- and *tagln*-double positive VSMCs. These results were consistent with those from a previous report using a *Tg(acta2:EGFP)* line that marks smooth muscle cells (Whitesell et al., 2014). However, EGFP-positive cells at the dorsal side of the DA did not exhibit RFP expression (Fig. S4B), suggesting that VSMCs at the dorsal part do not express *pdgfrb*. Thus, distinct types of VSMCs might be present on the dorsal and ventral sides of the DA.

Live imaging of MC coverage of ISVs

We then explored when and how ISVs become covered by MCs by analyzing *TgBAC(pdgfrb:EGFP);Tg(fli1a:Myr-mCherry)* zebrafish. The emergence of EGFP-positive cells around the ISVs started from 48 to 60 hpf (Fig. 5A,B). The number of EGFP-positive cells in the ISVs and the number of ISVs covered by EGFP-positive cells gradually increased until at least 120 hpf (Fig. 5A,B). EGFP-positive cells tended to extend their processes along the inter-EC junctions, as observed in the CtA (Fig. S4D,E). However, alignment of MC processes along the inter-EC junctions in ISVs was less

Development (2016) 143, 1328-1339 doi:10.1242/dev.132654

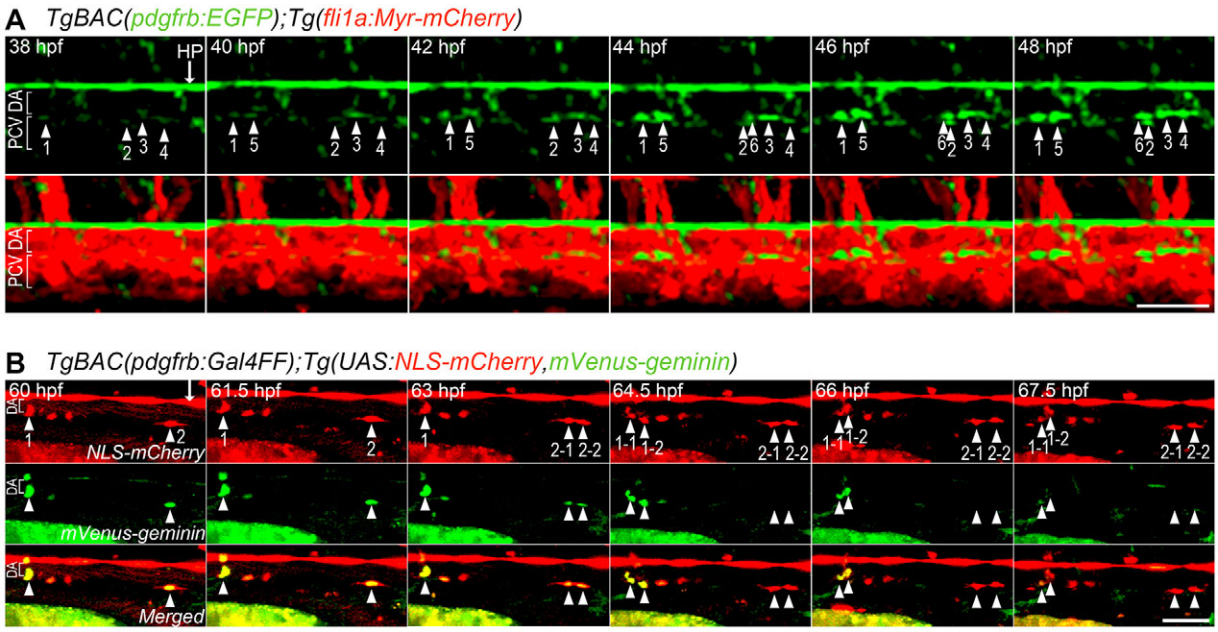

Fig. 4. Live imaging of MC coverage of axial vessels in the trunk. (A) Time-lapse confocal images of an axial vessel in the trunk of *TgBAC(pdgfrb:EGFP); Tg(fli1a:Myr-mCherry)* embryos (38-48 hpf). Upper, *pdgfrb:EGFP*; lower, merged images of *pdgfrb:EGFP* (green) and *fli1a:Myr-mCherry* (red). Arrowheads with numbers indicate individual EGFP-positive cells emerging at the ventral part of the DA. Arrow indicates hypochord (HP). (B) Time-lapse confocal images of a trunk axial vessel in *TgBAC(pdgfrb:Gal4FF);Tg(UAS:NLS-mCherry,mVenus-geminin)* embryo (60-67.5 hpf). Top, *NLS-mCherry* (red); middle, *mVenus-geminin* (the cells in the S/G2/M phase of the cell cycle) (green); bottom, merged images. Arrowheads with numbers indicate individual mCherry/mVenus double-positive cells located in the ventral part of DA. Note that mCherry/mVenus double-positive cells (1 and 2) divided into two daughter cells (1-1/1-2 and 2-1/2-2), which subsequently lost mVenus fluorescence. Arrow indicates hypochord. Lateral view, anterior to the left. Scale bars: 50 µm.

frequent than in CtA vessels, suggesting a diversity of MCs in different vascular beds. Time-lapse imaging analyses suggested two distinct modes of MC coverage of ISVs. One mechanism depended on recruitment of MCs that originally emerged in the ventral part of the DA. Some EGFP-positive cells located in the ventral side of the DA migrated dorsally to cover the ISVs (Fig. 5C; Movie 10). The other mechanism involved *de novo* formation of MCs around the ISVs. Indeed, the cells located in close proximity to the ISVs started to emit green fluorescence and contacted the ECs in the ISVs (Fig. 5D; Movie 10). Furthermore, the EGFP-positive cells around the ISVs frequently proliferated; therefore, it is possible that they contribute to the MC coverage of ISVs (Movie 10). These results indicate that MCs cover the ISVs in two ways, one relying on the recruitment of MCs from the DA and the other involving *de novo* differentiation of MCs in the ISVs followed by their proliferation.

The number of MCs covering ISVs increased during development (Fig. 5A). Nevertheless, ∼40% of the ISVs remained uncovered by MCs at 120 hpf (Fig. 5B), prompting us to hypothesize that MC coverage of ISVs might be affected by the difference between arteries and veins. To address this hypothesis, we counted separately the number of EGFP-positive cells in arterial ISVs (aISVs) and in venous ISVs (vISVs) in 120 hpf *TgBAC (pdgfrb:EGFP);Tg(fli1a:Myr-mCherry)* larvae (Fig. 5E-G). Most aISVs, but only 50% vISVs, were covered by EGFP-positive cells (Fig. 5F). The number of EGFP-positive cells around the aISVs was significantly greater than that around the vISVs (Fig. 5G). These results indicate that MCs preferentially cover aISVs compared with vISVs. However, despite this preferential coverage of aISVs with MCs, ∼50% vISVs was covered by MCs (Fig. 5F). In addition, we noticed that MCs covering the vISVs tended to be located in the dorsal part (Fig. 5E,H). As ECs located in the dorsal part of the vISVs are thought to be derived from the DA (Isogai et al., 2003), these ECs might maintain the arterial identity even though they exist in venous vessels. If this is the case, MCs might contact arterial ECs within the vISVs. Therefore, we analyzed *TgBAC(pdgfrb:EGFP); Tg(flt1:mCherry)* larvae, in which arterial ECs are visualized by mCherry fluorescence (Kwon et al., 2013). The dorsal part of the vISVs was weakly but clearly labeled by mCherry fluorescence, suggesting that ECs located in the dorsal region of vISVs retain arterial identity (Fig. 5I). Importantly, EGFP-positive cells preferentially adhered to *flt1* promoter-activated arterial ECs compared with venous ECs within the vISVs (Fig. 5I,J). Taken together with the evidence that MCs covered the DA, but not the PCV (Fig. 4A), these findings indicate that arterial ECs are preferentially covered by MCs during vascular development.

The preferential coverage of arterial ECs with MCs prompted us to hypothesize that arterial ECs might promote MC development. To test this hypothesis, we analyzed *kdrl* and *kdr* morphants that exhibited defective formation of the DA and aISVs, and found that MC development in the trunk was severely impaired in the absence of the DA and aISVs (Fig. S5A). These results suggest that arterial, but not venous, ECs play an instructive role in MC development. As functional characteristics of arteries and veins partly depend on differential levels of shear stress and pressure exerted by blood flow, blood flow might be involved in MC development. However, MCs covering the DA and ISVs were observed even in *tnnt2a* morphants that lack blood flow (Fig. S5B). Thus, arterial ECs might promote MC development in the trunk in a blood flow-independent manner.

We investigated further the role of Pdgfrβ signaling in MC development in the trunk vasculature. Neither *pdgfrb*$^{sa16389/sa16389}$ mutant nor AG1296-treated larvae showed apparent defects in trunk vessels (Fig. 5K; Fig. S5C,D). MCs covering the DA and ISVs were

Development (2016) 143, 1328-1339 doi:10.1242/dev.132654

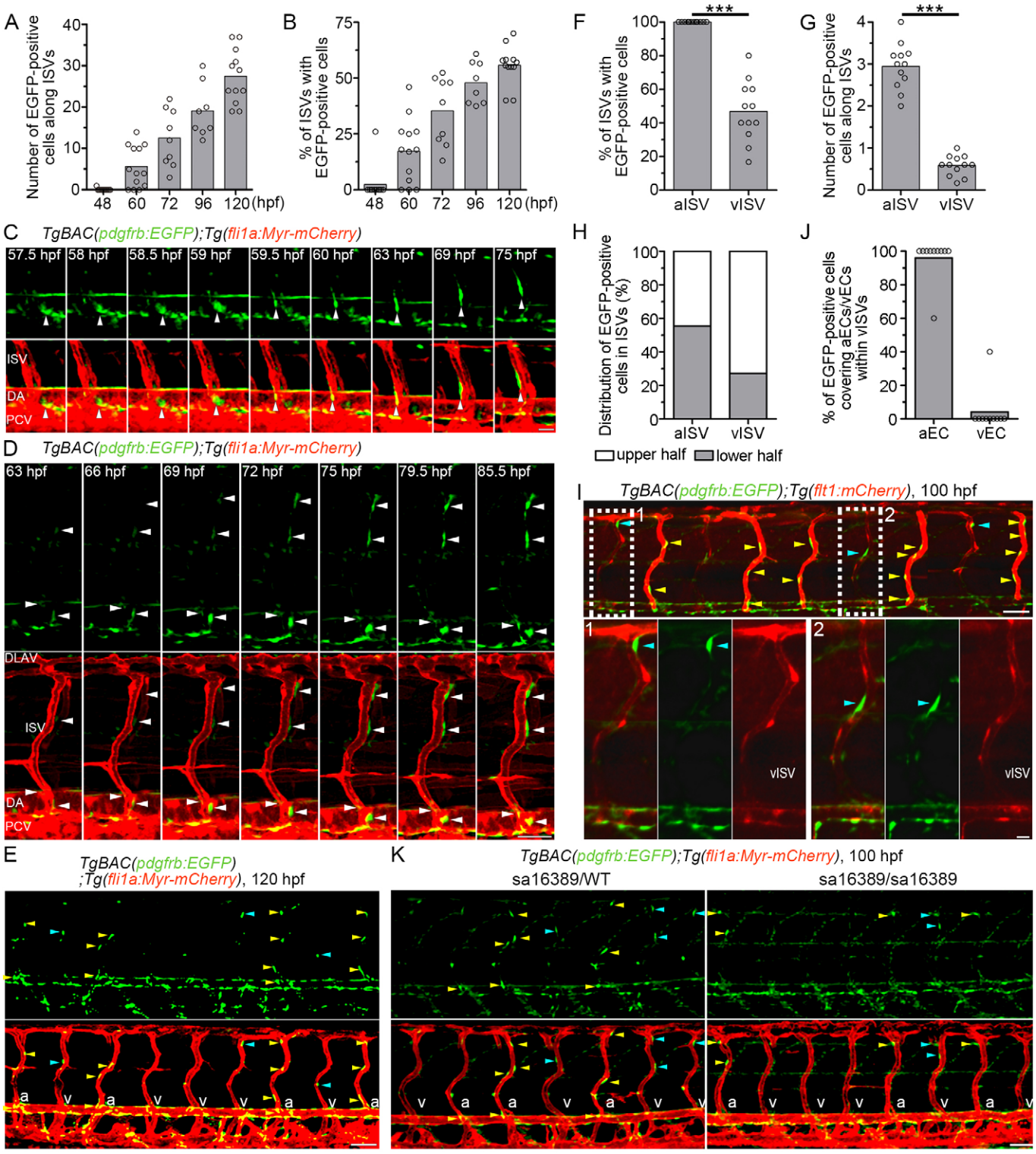

Fig. 5. See next page for legend.

detected even in the *pdgfrb*$^{sa16389/sa16389}$ mutant and AG1296-treated larvae, although the number of MCs was lower compared with *pdgfrb*$^{sa16389/WT}$ and control larvae, respectively (Fig. 5K; Fig. S5C,D). These findings indicate that Pdgfrβ-mediated signaling is not essential for the development of MCs covering the trunk vessels but might regulate their subsequent proliferation and recruitment.

Lineage tracing for identification of MC origins in zebrafish

MCs originate from neural crest cells and mesoderm (Majesky, 2007; Wasteson et al., 2008; Winkler et al., 2011). To analyze the origins of MCs in the zebrafish vasculature, we established *TgBAC(pdgfrb:Gal4FF);(UAS:loxP-mCherry-loxP-mVenus)* (*pdgfrb* reporter) fish and crossed with *Tg(sox10:Cre)* (Rodrigues et al., 2012) or *Tg(tbx6:Cre,myl7:EGFP)* (Lee et al., 2013) lines for

Development (2016) 143, 1328-1339 doi:10.1242/dev.132654

Fig. 5. Live imaging of MC coverage of ISVs. (A,B) The number of EGFP-positive cells covering mCherry-labeled ISVs (A) and the percentage of ISVs covered by more than one EGFP-positive cell (B) in the left side of *TgBAC (pdgfrb:EGFP);Tg(fli1a:Myr-mCherry)* embryos or larvae at the stages indicated below. ($n \geq 8$). (C) Time-lapse confocal images of the trunk vasculature in a *TgBAC(pdgfrb:EGFP);Tg(fli1a:Myr-mCherry)* embryo (57.5-75 hpf). Upper, *pdgfrb:EGFP*; lower, merged image of *pdgfrb:EGFP* (green) and *fli1a:Myr-mCherry* (red). Arrowheads indicate an EGFP-positive cell that initially located in the ventral part of DA and subsequently migrated towards the ISV. (D) Time-lapse confocal images of the trunk vasculature in a *TgBAC (pdgfrb:EGFP);Tg(fli1a:Myr-mCherry)* embryo (63-85.5 hpf), as in C. Arrowheads indicate EGFP-positive cells covering the ISVs. Note that the cells around the ISVs gradually emitted a stronger EGFP signal. (E) Confocal images of trunk vasculature in a *TgBAC(pdgfrb:EGFP);Tg(fli1a:Myr-mCherry)* larva at 120 hpf. Upper, *pdgfrb:EGFP*; lower, merged image of *pdgfrb:EGFP* (green) and *fli1a:Myr-mCherry* (red). Yellow and blue arrowheads indicate the EGFP-positive cells covering arterial ISVs (aISVs) and those covering venous ISVs (vISVs), respectively. 'a' and 'v' in the merged image indicate aISVs and vISVs, respectively. (F) Percentage of aISVs/vISVs covered by more than one EGFP-positive cell, as observed in E ($n \geq 12$). (G) The number of EGFP-positive cells covering aISVs/vISVs, as observed in E ($n \geq 12$). (H) Percentage of EGFP-positive cells covering the upper and lower half of aISVs/vISVs, as observed in E ($n=12$). (I) Confocal images of trunk vasculature in a *TgBAC (pdgfrb:EGFP);Tg(flt1:mCherry)* larva at 100 hpf. Fluorescence signal derived from *flt1:mCherry* labels arterial ECs (Bussmann et al., 2010). The merged image of *pdgfrb:EGFP* (green) and *flt1:mCherry* (red) is shown at the top. The boxed areas labeled 1 and 2 are enlarged at the bottom, showing the merged image of *pdgfrb:EGFP* and *flt1:mCherry* (left), *pdgfrb:EGFP* (center) and *flt1:mCherry* (right). Yellow and blue arrowheads indicate the EGFP-positive cells covering aISVs and those covering vISVs, respectively. Note that MCs adhered to the *flt1:mCherry*-positive arterial ECs within vISVs. (J) Percentage of EGFP-positive cells adhering to arterial ECs (aEC) and those adhering to venous ECs (vECs) within vISVs, as observed in I ($n=10$). (K) Confocal images of trunk vasculature of the *pdgfrb* heterozygous (sa16389/WT) and homozygous (sa16389/sa16389) larvae in the *TgBAC(pdgfrb:EGFP);Tg(fli1a:Myr-mCherry)* background at 100 hpf are shown, as in E. In A,B,F,G and J, bars and circles indicate averages and individual values, respectively. ***$P<0.001$. Lateral view, anterior to the left. DLAV, dorsal longitudinal anastomotic vessel; ISV, intersegmental vessel; DA, dorsal aorta; PCV, posterior cardinal vein; aISV, arterial ISV; vISV, venous ISV. Scale bars: 20 µm (C, enlarged images in I); 50 µm (D,E,I,K).

labeling the neural crest- or mesoderm-derived MCs with mVenus expression, respectively (Fig. 6A). Indeed, *pdgfrb* reporter larvae crossed with *Tg(sox10:Cre)* line exhibited mVenus fluorescence in the *pdgfrb* promoter-active neural crest-derived tissues, including iris, jaw and pharyngeal arch (Mongera et al., 2013; Rodrigues et al., 2012), suggesting that this lineage-tracing system works (Fig. 6B).

First, we determined the origin of MCs in the trunk vasculature. Most MCs in the trunk vasculature were labeled with mVenus expression in the *pdgfrb* reporter crossed with the *Tg(tbx6:Cre, myl7:EGFP)* line, but not in that crossed with the *Tg(sox10:Cre)* line (Fig. 6B,C). To identify the MC origin in the trunk vasculature, we analyzed *foxd3*/*tfap2a* double morphants, which exhibit defects in neural crest formation, and *tbx6*/*hand2* double morphants, in which the tissues derived from paraxial and lateral plate mesoderm fail to develop (Lee et al., 2009; Nikaido et al., 2002; Santoro et al., 2009; Wang et al., 2011). MC emergence in the DA and ISVs was severely impaired in the *tbx6*/*hand2* double morphant larvae but occurred normally in the *foxd3*/*tfap2a*-double morphant larvae (Fig. S6A,B). These results suggest that MCs in the trunk vessels are derived from the paraxial and lateral plate mesoderm.

Recently, Wang et al. have reported that zebrafish brain vessels contain neural crest-derived pericytes (Wang et al., 2014). However, it remains unknown whether all or specific types of brain vessels are covered by the neural crest-derived pericytes. Therefore, we addressed this question by analyzing our *pdgfrb* reporter line. When crossed with the *Tg(sox10:Cre)* line, *pdgfrb* reporter fish exhibited mVenus fluorescence in the anterior part of MMCtAs and in the CVP at the larval stage and in the forebrain at the juvenile stage (Fig. S7A,B; data not shown). Together with evidence that the MCs originally emerging around the CVP migrated to MMCtAs (Movie 4), these results suggest that neural crest-derived MCs develop around the CVP and migrate to cover the MMCtAs. Consistently, depletion of *foxd3*/*tfap2a* led to the reduction of *pdgfrb*-positive MCs in the CVP (Fig. S7C).

By contrast, the mVenus-positive MCs were hardly observed in the hindbrain vessels of the *pdgfrb* reporter line crossed with the *Tg(sox10:Cre)* line (Fig. 6D; Fig. S7A,B). In addition, MCs emerged around the BCA, PCS and BA even in the *foxd3*/*tfap2a* double morphant larvae, although the MC coverage of CtA was significantly impaired in these morphants (Fig. S7D-F). These results suggest that neural crest cells do not contribute to MC development in the base of the hindbrain but might be required for their subsequent recruitment into the CtA.

Thus, we investigated the contribution of mesodermal cells to the MC coverage of hindbrain vasculature and found that some of the *pdgfrb* reporter larvae crossed with the *Tg(tbx6:Cre,myl7:EGFP)* line showed mVenus-positive MCs in the hindbrain vessels (Fig. 6D; Fig. S7G,H). Because activity of the *tbx6* promoter used to express Cre recombinase is relatively low in the dorsal mesoderm, we also utilized the *no tail a* (*ntla*; *ta* – Zebrafish Information Network) promoter, which is active in the dorsal mesoderm (Goering et al., 2003; Lee et al., 2013). In *pdgfrb* reporter larvae injected with a plasmid (*ntla:Cre-2A-mCherry*), mVenus-positive MCs were detected not only in the trunk vessels but also in the hindbrain vessels (Fig. S7I), suggesting a mesodermal origin of MCs in the hindbrain vessels. We also analyzed *tbx6*/*hand2* double morphant larvae to confirm the mesodermal origin of MCs, but they exhibited severe defects in hindbrain vessels (Fig. S7J). However, *tbx6* morphants lacking paraxial mesoderm-derived tissues showed a decreased number of MCs covering the hindbrain vessels without apparent vascular defects (Fig. S7K-M). These results indicate that MCs in hindbrain vessels are mainly derived from the mesoderm. In addition, lineage-tracing studies and analyses of *foxd3*/*tfap2a* and *tbx6*/*hand2* double morphants revealed the neural crest origin of MCs in the hyaloid vessels (Fig. 6D; Fig. S8A,B).

Finally, we analyzed the origin of MCs covering vessels in the pharyngeal region. mVenus-positive MCs were detected in the hypobranchial artery (HA) and aortic arches (AAs) of *pdgfrb* reporter larvae crossed with the *Tg(sox10:Cre)* line, but not of those crossed with the *Tg(tbx6:Cre)* line (Fig. 6E). Consistently, *foxd3*/*tfap2a* double morphant and *foxd3* morphant larvae showed a decreased number of MCs covering the HA and AAs (Fig. S8C,D). These results indicate that the HA and AAs are covered by neural crest-derived MCs.

DISCUSSION

In this study, we succeeded for the first time in analyzing MC dynamics in living animals at single-cell resolution by generating zebrafish Tg lines that express fluorescent proteins and the Gal4FF driver under control of the *pdgfrb* promoter. By exploiting our Tg lines, we showed that MCs terminally differentiate around vessels, then actively proliferate and migrate along EC tubes, thereby covering entire vessels. In addition, our lineage-tracing analyses revealed that MCs in the trunk vasculature are derived from the mesoderm, whereas those in the head region have either neural crest or mesodermal origin.

Development (2016) 143, 1328-1339 doi:10.1242/dev.132654

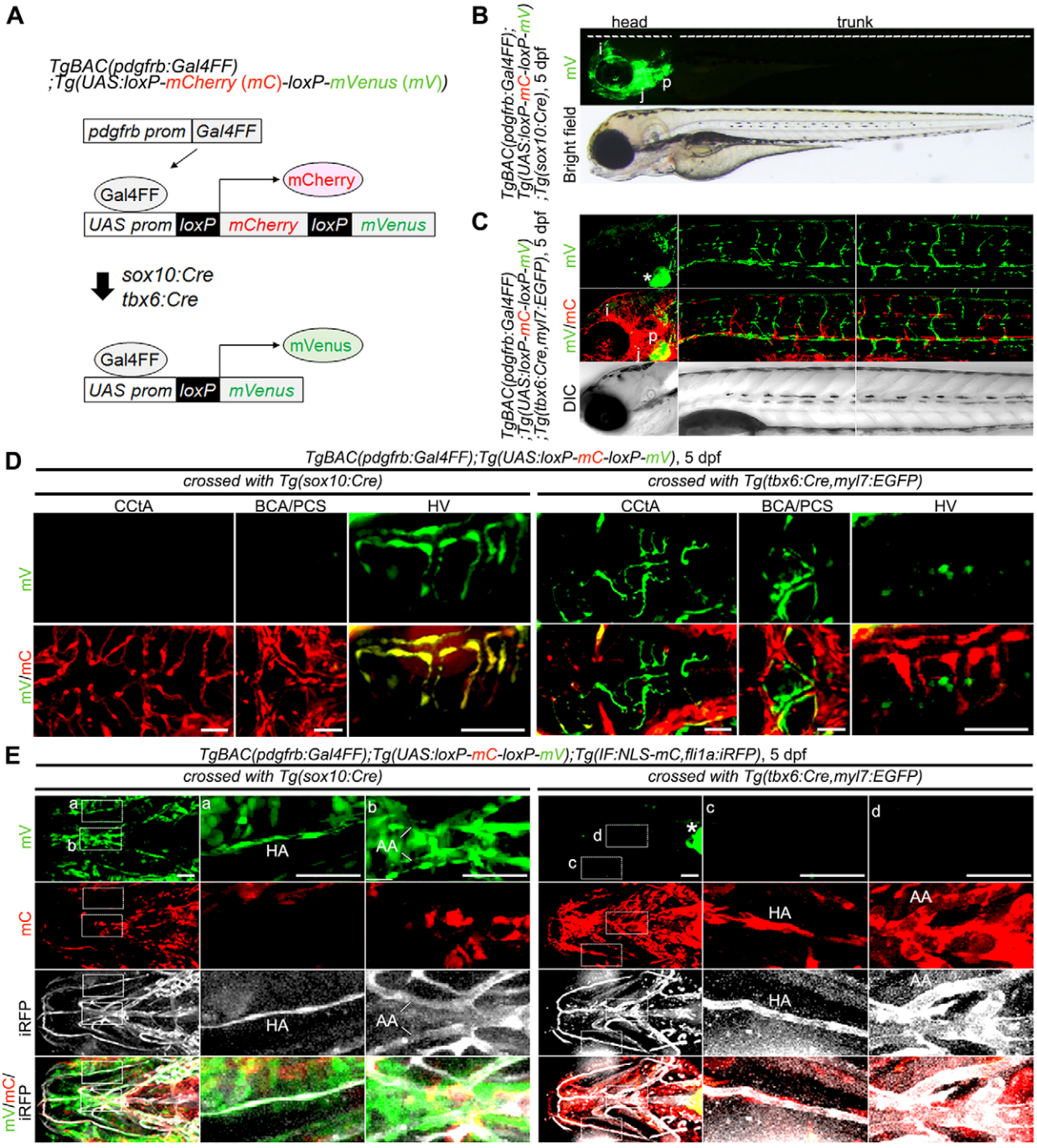

Fig. 6. Lineage tracing for identification of MC origins. (A) Schematic of the protocol used for lineage-tracing analysis. *TgBAC(pdgfrb:Gal4FF);Tg(UAS:loxP-mCherry* (*mC*)*-loxP-mVenus* (*mV*)*)* zebrafish (*pdgfrb* reporter) express mCherry in the *pdgfrb*-positive cells (top). In the *pdgfrb* reporter fish crossed with *Tg(sox10:Cre)* or *Tg(tbx6:Cre,myl7:EGFP)* line, the *sox10*-positive neural crest-derived MCs or *tbx6*-positive mesoderm-derived MCs, respectively, are labeled with mVenus expression because of Cre-mediated excision of *mCherry* gene flanked by loxP (bottom). (B) Lateral view of a *TgBAC(pdgfrb:Gal4FF);Tg(UAS:loxP-mC-loxP-mV);Tg(sox10:Cre)* larva at 5 dpf. Upper, mVenus; lower, brightfield image. (C) Confocal images of head (left column) and trunk (center and right columns) regions in a *TgBAC(pdgfrb:Gal4FF);Tg(UAS:loxP-mC-loxP-mV);Tg(tbx6:Cre,myl7:EGFP)* larva at 5 dpf. Upper, mVenus; middle, merged images of mVenus (green) and mCherry (red); lower, differential interference contrast (DIC) images. (D) Confocal images of head regions in a 5 dpf *TgBAC(pdgfrb:Gal4FF);Tg(UAS:loxP-mC-loxP-mV)* larva crossed with *Tg(sox10:Cre)* (left three columns) or *Tg(tbx6:Cre,myl7:EGFP)* (right three columns) fish lines. Dorsal view, anterior to the left. Images of CCtA, BCA/PCS and HV are shown in the left, center and right columns, respectively. Upper, mVenus; lower, the merged images of mVenus (green) and mCherry (red). Note that mVenus-labeled cells indicate *sox10*-positive neural crest-derived MCs (left three columns) or *tbx6*-positive mesoderm-derived MCs (right three columns). Scale bars: 50 µm (CCtA, HV); 20 µm (BCA/PCS). (E) Confocal images of pharyngeal regions in 5 dpf *TgBAC (pdgfrb:Gal4FF);Tg(UAS:loxP-mC-loxP-mV);Tg(IF:NLS-mCherry,fli1a:iRFP)* larvae crossed with *Tg(sox10:Cre)* (left three columns) or *Tg(tbx6:Cre,myl7:EGFP)* (right three columns) fish lines. The larvae expressing iRFP670 under the control of *fli1a* promoter were identified by *intestinal fatty acid binding protein* (*IF*; also known as *fabp2*) promoter-driven expression of NLS-mCherry in the intestine. Ventral view, anterior to the left. Boxed areas showing hypobranchial artery (HA) (a,c) and aortic arches (AA) (b,d) are enlarged to the right of the original images. Top row, mVenus; second row, mCherry; third row, *fli1a:iRFP* (iRFP); bottom row, merged images of mVenus (green), mCherry (red) and iRFP (white). Scale bars: 50 µm. Asterisks in C and E indicate heart visualized by *myl7:EGFP*. mC, mCherry; mV, mVenus; i, iris; j, jaw; p, pharyngeal arch.

Development (2016) 143, 1328-1339 doi:10.1242/dev.132654

Signaling from the arterial ECs might regulate terminal differentiation of MCs. MCs mainly covered arterial blood vessels, at least, until the larval stage. Similarly, preferential MC coverage of arterial vessels has been reported in mouse embryos (Hellstrom et al., 1999). Why is it mainly the arterial blood vessels that are surrounded by MCs? Our data showed that, although weakly EGFP-positive cells settled around both arterial and venous vessels in *Tg(pdgfrb:EGFP)* embryos, only the cells in close vicinity of arterial vessels differentiated into strongly EGFP-positive MCs. In addition, MC development was impaired by the defective formation of blood vessels. These findings suggest that signaling from arterial ECs, but not from venous ECs, promotes MC differentiation. Consistent with this, Jagged-1, which is preferentially expressed in the arterial vessels, promotes MC differentiation through activation of Notch 3 receptors (Armulik et al., 2011; Liu et al., 2009; Villa et al., 2001).

Arterial ECs might also promote expansion of differentiated MCs surrounding the arteries. EC-derived PDGF-B is known to induce proliferation and migration of PDGFRβ-expressing MCs during embryogenesis in mice (Hellstrom et al., 1999). Consistent with this, we observed that suppression of Pdgfrβ signaling inhibited MC coverage of CtA vessels, which depends on proliferation and migration of MCs originally emerging around the vessels in the cerebral base. Importantly, as endothelial expression of PDGF-B is restricted to the arteries and capillaries in the early stages of mouse development (Hellstrom et al., 1999), arterial EC-derived PDGF-B might regulate MC coverage of arterial vessels by inducing proliferation and migration of differentiated MCs.

Coverage of the DA with VSMCs occurs through a complex mechanism. Consistent with our lineage-tracing analyses, previous studies in zebrafish, quail and mice have also suggested the mesodermal origin of VSMCs in the DA (Santoro et al., 2009; Wasteson et al., 2008; Wiegreffe et al., 2007). However, VSMCs in the DA might have a heterogeneous cellular origin. At 7 dpf, *tagln*-positive cells in the ventral side of the DA were *pdgfrb*-positive, whereas those in the dorsal side did not express *pdgfrb*, suggesting that VSMCs in the dorsal and ventral sides of the DA have distinct origins. Consistent with this, it has been reported that lateral plate mesoderm-derived VSMCs cover the ventral side of the descending DA in the early stage of aortic development in mice, whereas the VSMCs covering the dorsal side are derived from the somites (Wasteson et al., 2008).

In zebrafish, MCs covering the cranial vessels originated from both mesoderm and neural crest cells. To date, contribution of neural crest cells to brain MCs has been demonstrated in vertebrates including mice, bird and zebrafish (Etchevers et al., 2001; Heglind et al., 2005; Korn et al., 2002; Trost et al., 2013; Wang et al., 2014; Yamanishi et al., 2012). In agreement with this, our analyses indicated a neural crest origin of MCs in the anterior part of the brain and in the hyaloid vessels. However, our data also revealed a mesodermal origin of MCs in hindbrain vessels. Two groups have previously analyzed the origins of MCs in avian brain and have reported discrepant results. Consistent with our observation, Etchevers et al. have reported that MCs in the forebrain are derived from neural crest cells, whereas those of mesodermal origin cover the vessels in the posterior part of brain (Etchevers et al., 2001). By contrast, Korn et al. have reported that neuroectoderm can give rise to MCs in all the vessels in the brain (Korn et al., 2002). Thus, further careful examinations are required to identify the presence of mesoderm-derived MCs in the brain.

MCs migrate along inter-EC junctions during their coverage of blood vessels. During MC coverage of the CtA, MCs extend their processes along inter-EC junctions and subsequently relocate their cell bodies to the scaffold structures formed within the proceeding processes in order to move forward. It is known that substrate stiffness largely influences cell migration. Indeed, recent studies have shown that many different types of cells, including VSMCs, move towards stiffer substrates (Isenberg et al., 2009). Therefore, inter-EC junctions might provide the rigid scaffold required for efficient MC migration, because inter-EC junctions are supported by the actin cytoskeleton (Ando et al., 2013; Phng et al., 2015). Alternatively, N-cadherin (Cadherin 2) might regulate MC migration along inter-EC junctions. In ECs, vascular endothelial-cadherin (Cadherin 5) mediates EC-EC junctions, whereas N-cadherin is thought to regulate cell adhesion between MCs and ECs. However, a previous study has also reported that N-cadherin partially localizes to inter-EC junctions in addition to its plasma membrane localization (Luo and Radice, 2005). Therefore, N-cadherin expressed by MCs might interact with N-cadherin localized at the inter-EC junctions to mediate MC migration along the inter-EC junctions. However, further studies are needed to clarify the mechanism by which MCs migrate along inter-EC junctions and its biological significance.

Here, we have successfully uncovered the mechanism underlying MC coverage of blood vessels by establishing novel zebrafish lines for *in vivo* visualization of MCs. Thus, Tg lines that we have developed in this study will substantially contribute to our understanding of MC biology.

MATERIALS AND METHODS

Zebrafish husbandry

Zebrafish (*Danio rerio*) were maintained as previously described (Fukuhara et al., 2014). Embryos and larvae were staged by hpf at 28°C (Kimmel et al., 1995).

Plasmid construction and BAC recombineering

Construction of the Tol2 vectors used to generate transgenic zebrafish lines is described in supplementary Materials and Methods. BAC clones encoding EGFP, mCherry or Gal4FF under *pdgfrb* promoter were prepared as described in supplementary Materials and Methods according to the method described in a previous report (Bussmann and Schulte-Merker, 2011).

Transgenic and mutant zebrafish lines

The Tol2 transposon system was used to generate transgenic zebrafish lines as described in supplementary Materials and Methods. *pdgfrb*^{sa16389} mutant zebrafish were obtained from the European Zebrafish Resource Center.

Image acquisition and processing

Embryos and larvae were anesthetized and mounted in 1% low-melting agarose on a 35-mm diameter glass-based dish (Asahi Techno Glass, Shizuoka, Japan), as previously described (Fukuhara et al., 2014).

Confocal images were obtained using a FluoView FV1000 or FV1200 confocal upright microscope (Olympus, Tokyo, Japan) equipped with a water-immersion 20× (XLUMPlanFL, 1.0 NA) lens. The 473 nm, 559 nm and 633 nm laser lines were employed. Obtained confocal images were processed using Olympus Fluoview (FV10-ASW) or FluoRender (http://www.fluorender.org). Images processed with FluoRender were shown in FluoRender composite mode in which deeper objections became visible.

Fluorescence and brightfield images were taken with a fluorescence stereozoom microscope (SZX12, Olympus).

FACS and RT-PCR

EGFP-negative/mCherry negative, EGFP-positive/mCherry negative and EGFP-negative/mCherry-positive cells were isolated from *TgBAC(pdgfrb:EGFP);Tg(fli1a:Myr-mCherry)* larvae by FACS and subjected to RT-PCR analyses as described in supplementary Materials and Methods.

Development (2016) 143, 1328-1339 doi:10.1242/dev.132654

Immunohistochemistry

TgBAC(pdgfrb:EGFP);Tg(fli1a:Myr-mCherry) and *TgBAC(tagln:EGFP);Tg(fli1a:Myr-mCherry)* juvenile zebrafish were subjected to immunohistochemistry with anti-α-SMA antibody at 1:300 as described in supplementary Materials and Methods.

Quantification

To quantify MC processes following the inter-EC junctions, we measured the total length of each process extended by MCs (X) and the length of the corresponding process that aligned along the Pecam1-EGFP-labeled inter-EC junctions (Y). Alignment of MC processes along the inter-EC junctions was expressed as a percentage of total length (X/Y×100).

Injections of morpholino oligonucleotides

For morpholino oligonucleotide (MO)-mediated knockdown, embryos were injected at one-cell stage with the MOs indicated in supplementary Materials and Methods.

Statistical analysis

Data are expressed as means±s.e.m. Statistical significance was determined by a Student's *t*-test for paired samples or one-way analysis of variance with Turkey's test for multiple comparisons. Data were considered statistically significant if P-values <0.05.

Acknowledgements

We thank S. Schulte-Merker for providing information and plasmids for BAC recombineering; K. Kawakami for the Tol2 system and the *Tg(UAS:GFP)* and *Tg(UAS:RFP)* lines; T. J. Carney for the *Tg(tbx6:Cre,myl7:EGFP)*^{sq6} line; G. Felsenfeld for the pJC13-1; and A. Sakakibara for the iRFP670. We are grateful to M. Sone, T. Babazono, W. Koeda, K. Hiratomi and E. Okamoto for technical assistance. This work was made possible in part by software funded by the NIH: FluoRender: An Imaging Tool for Visualization and Analysis of Confocal Data as Applied to Zebrafish Research [R01-GM098151-01].

Competing interests

The authors declare no competing or financial interests.

Author contributions

K.A., S.F. and N.M. conceived, designed the research and wrote the manuscript. K.A. performed the experiments and analyzed the results. N.I. conceived the research. H.N. and H.F. supported the experiments. R.N.K. developed *Tg(sox10:Cre)* line.

Funding

This work was supported in part by Grants-in-Aid for Scientific Research on Innovative Areas 'Fluorescence Live Imaging' [No. 22113009 to S.F.] and 'Neuro-Vascular Wiring' [No. 22122003 to N.M.] from The Ministry of Education, Culture, Sports, Science, and Technology, Japan; by Grants-in-Aid for Young Scientists (Start-up) [No. 26893336 to K.A.], for Scientific Research (B) [No. 25293050 to S.F. and No. 24370084 to N.M.], and for Exploratory Research [No. 26670107 to S.F.] from the Japan Society for the Promotion of Science; and by grants from the Ministry of Health, Labour, and Welfare of Japan [KHC1103 to N.M.]; the Core Research for Evolutional Science and Technology (CREST) program of the Japan Agency for Medical Research and Development (AMED) [15652238 to N.M.]; Precursory Research for Innovative Medical Care (PRIME), AMED [15665521 to S.F.]; the Takeda Science Foundation (S.F., N.M.); the Naito Foundation (S.F.); Mochida Memorial Foundation for Medical and Pharmaceutical Research (S.F.); the Daiichi Sankyo Foundation of Life Science (S.F.); and the Medical Research Council [MR/J001457/1 to R.N.K.]. Deposited in PMC for release after 6 months.

Supplementary information

Supplementary information available online at
http://dev.biologists.org/lookup/suppl/doi:10.1242/dev.132654/-/DC1

References

Ando, K., Fukuhara, S., Moriya, T., Obara, Y., Nakahata, N. and Mochizuki, N. (2013). Rap1 potentiates endothelial cell junctions by spatially controlling myosin II activity and actin organization. *J. Cell Biol.* **202**, 901-916.

Armulik, A., Genove, G. and Betsholtz, C. (2011). Pericytes: developmental, physiological, and pathological perspectives, problems, and promises. *Dev. Cell* **21**, 193-215.

Asakawa, K., Suster, M. L., Mizusawa, K., Nagayoshi, S., Kotani, T., Urasaki, A., Kishimoto, Y., Hibi, M. and Kawakami, K. (2008). Genetic dissection of neural circuits by Tol2 transposon-mediated Gal4 gene and enhancer trapping in zebrafish. *Proc. Natl. Acad. Sci. USA* **105**, 1255-1260.

Bussmann, J. and Schulte-Merker, S. (2011). Rapid BAC selection for tol2-mediated transgenesis in zebrafish. *Development* **138**, 4327-4332.

Bussmann, J., Bos, F. L., Urasaki, A., Kawakami, K., Duckers, H. J. and Schulte-Merker, S. (2010). Arteries provide essential guidance cues for lymphatic endothelial cells in the zebrafish trunk. *Development* **137**, 2653-2657.

Etchevers, H. C., Vincent, C., Le Douarin, N. M. and Couly, G. F. (2001). The cephalic neural crest provides pericytes and smooth muscle cells to all blood vessels of the face and forebrain. *Development* **128**, 1059-1068.

Foo, S. S., Turner, C. J., Adams, S., Compagni, A., Aubyn, D., Kogata, N., Lindblom, P., Shani, M., Zicha, D. and Adams, R. H. (2006). Ephrin-B2 controls cell motility and adhesion during blood-vessel-wall assembly. *Cell* **124**, 161-173.

French, C. R., Seshadri, S., Destefano, A. L., Fornage, M., Arnold, C. R., Gage, P. J., Skarie, J. M., Dobyns, W. B., Millen, K. J., Liu, T. et al. (2014). Mutation of FOXC1 and PITX2 induces cerebral small-vessel disease. *J. Clin. Invest.* **124**, 4877-4881.

Fujita, M., Cha, Y. R., Pham, V. N., Sakurai, A., Roman, B. L., Gutkind, J. S. and Weinstein, B. M. (2011). Assembly and patterning of the vascular network of the vertebrate hindbrain. *Development* **138**, 1705-1715.

Fukuhara, S., Zhang, J., Yuge, S., Ando, K., Wakayama, Y., Sakaue-Sawano, A., Miyawaki, A. and Mochizuki, N. (2014). Visualizing the cell-cycle progression of endothelial cells in zebrafish. *Dev. Biol.* **393**, 10-23.

Gaengel, K., Genove, G., Armulik, A. and Betsholtz, C. (2009). Endothelial-mural cell signaling in vascular development and angiogenesis. *Arterioscler. Thromb. Vasc. Biol.* **29**, 630-638.

Garg, N., Khunger, M., Gupta, A. and Kumar, N. (2014). Optimal management of hereditary hemorrhagic telangiectasia. *J. Blood Med.* **5**, 191-206.

Goering, L. M., Hoshijima, K., Hug, B., Bisgrove, B., Kispert, A. and Grunwald, D. J. (2003). An interacting network of T-box genes directs gene expression and fate in the zebrafish mesoderm. *Proc. Natl. Acad. Sci. USA* **100**, 9410-9415.

Heglind, M., Cederberg, A., Aquino, J., Lucas, G., Ernfors, P. and Enerback, S. (2005). Lack of the central nervous system- and neural crest-expressed forkhead gene Foxs1 affects motor function and body weight. *Mol. Cell. Biol.* **25**, 5616-5625.

Hellstrom, M., Kalen, M., Lindahl, P., Abramsson, A. and Betsholtz, C. (1999). Role of PDGF-B and PDGFR-beta in recruitment of vascular smooth muscle cells and pericytes during embryonic blood vessel formation in the mouse. *Development* **126**, 3047-3055.

Isenberg, B. C., Dimilla, P. A., Walker, M., Kim, S. and Wong, J. Y. (2009). Vascular smooth muscle cell durotaxis depends on substrate stiffness gradient strength. *Biophys. J.* **97**, 1313-1322.

Isogai, S., Lawson, N. D., Torrealday, S., Horiguchi, M. and Weinstein, B. M. (2003). Angiogenic network formation in the developing vertebrate trunk. *Development* **130**, 5281-5290.

Joutel, A., Corpechot, C., Ducros, A., Vahedi, K., Chabriat, H., Mouton, P., Alamowitch, S., Domenga, V., Cecillion, M., Marechal, E. et al. (1996). Notch3 mutations in CADASIL, a hereditary adult-onset condition causing stroke and dementia. *Nature* **383**, 707-710.

Kimmel, C. B., Ballard, W. W., Kimmel, S. R., Ullmann, B. and Schilling, T. F. (1995). Stages of embryonic development of the zebrafish. *Dev. Dyn.* **203**, 253-310.

Korn, J., Christ, B. and Kurz, H. (2002). Neuroectodermal origin of brain pericytes and vascular smooth muscle cells. *J. Comp. Neurol.* **442**, 78-88.

Kwon, H.-B., Fukuhara, S., Asakawa, K., Ando, K., Kashiwada, T., Kawakami, K., Hibi, M., Kwon, Y.-G., Kim, K.-W., Alitalo, K. et al. (2013). The parallel growth of motoneuron axons with the dorsal aorta depends on Vegfc/Vegfr3 signaling in zebrafish. *Development* **140**, 4081-4090.

Lee, H.-C., Tseng, W.-A., Lo, F.-Y., Liu, T.-M. and Tsai, H.-J. (2009). FoxD5 mediates anterior-posterior polarity through upstream modulator Fgf signaling during zebrafish somitogenesis. *Dev. Biol.* **336**, 232-245.

Lee, R. T. H., Knapik, E. W., Thiery, J. P. and Carney, T. J. (2013). An exclusively mesodermal origin of fin mesenchyme demonstrates that zebrafish trunk neural crest does not generate ectomesenchyme. *Development* **140**, 2923-2932.

Liu, H., Kennard, S. and Lilly, B. (2009). NOTCH3 expression is induced in mural cells through an autoregulatory loop that requires endothelial-expressed JAGGED1. *Circ. Res.* **104**, 466-475.

Luo, Y. and Radice, G. L. (2005). N-cadherin acts upstream of VE-cadherin in controlling vascular morphogenesis. *J. Cell Biol.* **169**, 29-34.

Majesky, M. W. (2007). Developmental basis of vascular smooth muscle diversity. *Arterioscler. Thromb. Vasc. Biol.* **27**, 1248-1258.

Mongera, A., Singh, A. P., Levesque, M. P., Chen, Y.-Y., Konstantinidis, P. and Nusslein-Volhard, C. (2013). Genetic lineage labeling in zebrafish uncovers novel neural crest contributions to the head, including gill pillar cells. *Development* **140**, 916-925.

Nikaido, M., Kawakami, A., Sawada, A., Furutani-Seiki, M., Takeda, H. and Araki, K. (2002). Tbx24, encoding a T-box protein, is mutated in the zebrafish somite-segmentation mutant fused somites. *Nat. Genet.* **31**, 195-199.

Development (2016) 143, 1328-1339 doi:10.1242/dev.132654

Olson, L. E. and Soriano, P. (2011). PDGFRbeta signaling regulates mural cell plasticity and inhibits fat development. *Dev. Cell* **20**, 815-826.

Phng, L.-K., Gebala, V., Bentley, K., Philippides, A., Wacker, A., Mathivet, T., Sauteur, L., Stanchi, F., Belting, H.-G., Affolter, M., et al. (2015). Formin-mediated actin polymerization at endothelial junctions is required for vessel lumen formation and stabilization. *Dev. Cell* **32**, 123-132.

Robin, Y.-M., Penel, N., Perot, G., Neuville, A., Velasco, V., Ranchere-Vince, D., Terrier, P. and Coindre, J.-M. (2013). Transgelin is a novel marker of smooth muscle differentiation that improves diagnostic accuracy of leiomyosarcomas: a comparative immunohistochemical reappraisal of myogenic markers in 900 soft tissue tumors. *Mod. Pathol.* **26**, 502-510.

Rodrigues, F. S. L. M., Doughton, G., Yang, B. and Kelsh, R. N. (2012). A novel transgenic line using the Cre-lox system to allow permanent lineage-labeling of the zebrafish neural crest. *Genesis* **50**, 750-757.

Sakaue-Sawano, A., Kurokawa, H., Morimura, T., Hanyu, A., Hama, H., Osawa, H., Kashiwagi, S., Fukami, K., Miyata, T., Miyoshi, H. et al. (2008). Visualizing spatiotemporal dynamics of multicellular cell-cycle progression. *Cell* **132**, 487-498.

Santoro, M. M., Pesce, G. and Stainier, D. Y. (2009). Characterization of vascular mural cells during zebrafish development. *Mech. Dev.* **126**, 638-649.

Seiler, C., Abrams, J. and Pack, M. (2010). Characterization of zebrafish intestinal smooth muscle development using a novel sm22alpha-b promoter. *Dev. Dyn.* **239**, 2806-2812.

Trost, A., Schroedl, F., Lange, S., Rivera, F. J., Tempfer, H., Korntner, S., Stolt, C. C., Wegner, M., Bogner, B., Kaser-Eichberger, A. et al. (2013). Neural crest origin of retinal and choroidal pericytes. *Invest. Ophthalmol. Vis. Sci.* **54**, 7910-7921.

Villa, N., Walker, L., Lindsell, C. E., Gasson, J., Iruela-Arispe, M. L. and Weinmaster, G. (2001). Vascular expression of Notch pathway receptors and ligands is restricted to arterial vessels. *Mech. Dev.* **108**, 161-164.

Wang, W.-D., Melville, D. B., Montero-Balaguer, M., Hatzopoulos, A. K. and Knapik, E. W. (2011). Tfap2a and Foxd3 regulate early steps in the development of the neural crest progenitor population. *Dev. Biol.* **360**, 173-185.

Wang, Y., Pan, L., Moens, C. B. and Appel, B. (2014). Notch3 establishes brain vascular integrity by regulating pericyte number. *Development* **141**, 307-317.

Wasteson, P., Johansson, B. R., Jukkola, T., Breuer, S., Akyurek, L. M., Partanen, J. and Lindahl, P. (2008). Developmental origin of smooth muscle cells in the descending aorta in mice. *Development* **135**, 1823-1832.

Whitesell, T. R., Kennedy, R. M., Carter, A. D., Rollins, E.-L., Georgijevic, S., Santoro, M. M. and Childs, S. J. (2014). An alpha-smooth muscle actin (acta2/alphasma) zebrafish transgenic line marking vascular mural cells and visceral smooth muscle cells. *PLoS ONE* **9**, e90590.

Wiegreffe, C., Christ, B., Huang, R. and Scaal, M. (2007). Sclerotomal origin of smooth muscle cells in the wall of the avian dorsal aorta. *Dev. Dyn.* **236**, 2578-2585.

Wiens, K. M., Lee, H. L., Shimada, H., Metcalf, A. E., Chao, M. Y. and Lien, C.-L. (2010). Platelet-derived growth factor receptor beta is critical for zebrafish intersegmental vessel formation. *PLoS ONE* **5**, e11324.

Winkler, E. A., Bell, R. D. and Zlokovic, B. V. (2011). Central nervous system pericytes in health and disease. *Nat. Neurosci.* **14**, 1398-1405.

Yamanishi, E., Takahashi, M., Saga, Y. and Osumi, N. (2012). Penetration and differentiation of cephalic neural crest-derived cells in the developing mouse telencephalon. *Dev. Growth Differ.* **54**, 785-800.

MATERIAL AND METHODS

Plasmids

The Tol2 vector system was kindly provided by K. Kawakami (National Institute of Genetics, Japan) (Kawakami et al., 2004; Urasaki et al., 2006). Tol2_amp and pCS2_Gal4FF_KanR vector for BAC recombineering were kindly provided by S. Schulte-Merker (University of Münster, Germany). pCS2_EGFP_KanR or pCS2_mCherry_KanR was generated by replacing Gal4FF in pCS2_Gal4FF_KanR vector with a PCR-amplified EGFP or mCherry cDNA.

A cDNA encoding nuclear localization signal (NLS)-tagged mCherry was amplified by PCR using pTolflk1-NLS-mCherry vector as a template (Fukuhara et al., 2014) and subcloned into the pTol2-E1b-UAS-E1b vector to construct the pTol2-NLS-mCherry-E1b-UAS-E1b plasmid. To generate the pTol2-UAS:NLS-mCherry, mVenus-geminin plasmid, a cDNA encoding mVenus fused to the N-terminal 100 aa of zebrafish geminin (mVenus-geminin) was amplified by PCR using pTolflk1-mVenus-zGem (1/100) plasmid as a template (Fukuhara et al., 2014) and subsequently inserted into the pTol2-NLS-mCherry-E1b-UAS-E1b vector.

To construct the plasmid encoding Pecam1-EGFP, a cDNA encoding full length of zebrafish *pecam1* (NM_001113799) was amplified by PCR using cDNA library derived from zebrafish embryos as a template and cloned into pEGFP-C1 vector (Clontech, Takara Bio Inc., Shiga, Japan). The pecam1-EGFP cDNA was subcloned into pTol2-fli1a vector (Fukuhara et al., 2014) to generate pTol2-fli1a-pecam1-EGFP plasmid.

To construct the plasmid encoding pTol2-5xUAS-loxP-mCherry-loxP-mVenus, two oligonucleotides encoding loxP sequence (ataacttcgtatagcatacattatacgaagttat) were

inserted into the pcDNA3.1 vector (Invitrogen, Carlsbad, CA). Then, a cDNA encoding mCherry and that expressing mVenus were PCR-amplified and sequentially inserted between two loxP sites and downstream of the second loxP site to generate the pcDNA3.1-loxP-mCherry-loxP-mVenus, respectively. Finally, the loxP-mCherry-loxP-mVenus cDNA was subcloned into the pTol2-5xUAS vector, a gift from K. Kawakami (National Institute of Genetics, Japan) (Asakawa et al., 2008; Distel et al., 2009), to generate the pTol2-5xUAS-loxP-mCherry-loxP-mVenus.

For construction of pTol2-IF-NLS-mCherry-HS4-fli-iRFP plasmid, PCR-amplified cDNA encoding NLS-tagged mCherry was subcloned into pTol2 vector to construct pTol2-NLS-mCherry. Then, a cDNA encoding the chicken β-globin insulator (HS4) was amplified by PCR using pJC13-1 vector, a gift from G. Felsenfeld (National Institute of Health, USA) (Yusufzai and Felsenfeld, 2004), as a template and subcloned into the pTol2-NLS-mCherry vector to generate pTol2-NLS-mCherry-HS4. To construct pTol2-NLS-mCherry-HS4-fli1a, a cDNA encoding fli1a promoter was PCR-amplified using pTol2-fli1a vector (Fukuhara et al., 2014) as a template and inserted downstream of HS4 insulator in the pTol2-NLS-mCherry-HS4 vector. Subsequently, a cDNA encoding -4.5 kb intestinal fatty acid binding protein (IF) promoter region (Her et al., 2004) was amplified by PCR using genomic DNA derived from zebrafish embryos as a template and 5'- aaagagactgaaagggcagaagcacagg-3' and 5'- gatgatgacagactgttgtgtgatc-3' primers. This DNA was subcloned into the upstream of NLS-mCherry in the pTol2-NLS-mCherry-HS4-fli1a vector to generate pTol2-IF-NLS-mCherry-HS4-fli1a. Finally, a pTol2-IF-NLS-mCherry-HS4-fli-iRFP plasmid was constructed by inserting a PCR-amplified cDNA encoding iRFP670, a gift from A. Sakakibara (Chubu University, Japan), into the downstream of fli1a promoter in the pTol2-IF-NLS-mCherry-HS4-fli1a

vector.

A cDNA encoding Cre recombinase (Kogata et al., 2006) followed by 2A peptide and mCherry was subcloned into pTol2-fli1a vector to generate pTol2-Cre-2A-mCherry. Then, a cDNA encoding -2.1 kb ntla promoter region was amplified by PCR using genomic DNA derived from zebrafish embryos as a template and 5'-TAACGCGTATACAATTCCTTTGTGCTGTTGCAACAC-3' and 5'-ATGCTAGCATTTCCGATCAAATAAAGCTTGAGAT-3' primers, and subcloned into the pTol2-Cre-2A-mCherry vector to generate pTol2-ntla-Cre-2A-mCherry.

BAC recombineering

pRedET plasmid (GeneBridge, Heidelberg, Germany) was introduced into E. coli containing either CH1073-606I16 BAC clone encoding *pdgfrb* gene (BacPAC resources, Oakland, CA) or CH1073-307D13 BAC clone encoding *tagln* gene by electroporation (1800 V, 25 μF, 200 Ω) to increase the efficiency of homologous recombination. Next, two Tol2 long terminal repeats in opposing directions flanking an ampicillin resistance cassette was amplified by PCR using Tol2_amp as a template and were inserted into the BAC vector backbone. Then, the cDNA encoding either EGFP, mCherry or Gal4FF together with a kanamycin resistance cassette (EGFP_KanR, mCherry_KanR or Gal4FF_KanR) was amplified by PCR using pCS2_EGFP_KanR, pCS2_mCherry_KanR or pCS2_Gal4FF_KanR plasmid as a template, respectively, and inserted at the start ATG of the *pdgfrb* or *tagln* gene. Primers to amplify the EGFP_KanR, mCherry_KanR or Gal4FF_KanR PCR product are as follows:

EGFP_KanR for CH1073-606I16,

5'-tgttgttttctctccgtctgcagtgttgaatgtgtcctgctctagaagaaACCATGGTGAGCAAGGGCGAG

GAG-3' and

5'-ttgtgatagcagtgaataggaagtggatgcggctgatggtcgaactcttTCAGAAGAACTCGTCAAGA AGGCG-3'; To amplify the mCherry_KanR for CH1073-606I16, the same primer pair for EGFP_KanR for CH1073-606I16 was used; Gal4FF_KanR for CH1073-606I16, 5'-tgttgttttctctccgtctgcagtgttgaatgtgtcctgctctagaagaaACCATGAAGCTACTGTCTTCTA TCGAAC-3' and

5'-ttgtgatagcagtgaataggaagtggatgcggctgatggtcgaactcttTCAGAAGAACTCGTCAAGA AGGCG-3'; EGFP_KanR for CH1073-307D13,

5'-atcacaggtgtttctctgtggacgctctgctgtttctccatcagggagcgACCATGGTGAGCAAGGGCGA GGAG-3' and

5'-atcttatcctgcacctgccggctcagcccataagacggccccttgtttgcTCAGAAGAACTCGTCAAGA AGGCG-3' (lowercase; homology arm to BAC vector. uppercase; primer binding site to the template plasmid).

Transgenic and mutant zebrafish lines

Tol2 transposase mRNA was *in vitro* transcribed with SP6 RNA polymerase from NotI-linearised pCS-TP vector using the mMESSAGE mMACHINE kit (Ambion, Austin, TX). To generate the *TgBAC(pdgfrb:EGFP)*^{ncv22}, *TgBAC(pdgfrb:mCherry)*^{ncv23}, *TgBAC(pdgfrb:Gal4FF)*^{ncv24} and *TgBAC(tagln:EGFP)*^{ncv25} zebrafish lines, the corresponding BAC DNA was co-injected with Tol2 transposase mRNA into one-cell stage embryos of wild type strain, AB. To establish the *Tg(UAS:NLS-mCherry,mVenus-geminin)*^{ncv26}, *Tg(fli1a:pecam1-EGFP)*^{ncv27}, *Tg(UAS:loxP-mCherry-loxP-mVenus)*^{ncv28} and *Tg(IF:NLS-mCherry,fli1a:iRFP)*^{ncv29} zebrafish lines, pTol2-UAS:NLS-mCherry,mVenus-geminin, pTol2-fli1a-pecam1-EGFP,

pTol2-5UAS-loxP-mCherry-loxP-mVenus and pTol2-IF-NLS-mCherry-HS4-fli1a-iRFP plasmids were injected along with Tol2 transposase mRNA into one-cell stage embryos, respectively. *Tg(UAS:GFP)* and *Tg(UAS:RFP)* fish lines were kindly provided by K. Kawakami (National Institute of Genetics, Japan) (Asakawa et al., 2008). *Tg(tbx6:Cre,myl7:EGFP)*^{sq6} fish was kindly provided by T. J. Carney (Agency for Science, Technology and Research, Singapore) (Lee et al., 2013). *Tg(sox17:DsRed)*^{s903} fish was obtained from the Zebrafish International Resource Center (University of Oregon, OR, USA). *Tg(fli1a:Myr-mCherry)*^{ncv1}, *Tg(fli1a:Myr-EGFP)*^{ncv2} (Fukuhara et al., 2014), *Tg(flt1:mCherry)*^{ncv30} (Kwon et al., 2013) and *Tg(sox10:Cre)*^{ba74} (Rodrigues et al., 2012) fish lines were previously described. Throughout the text, all Tg lines used in this study are simply described without their line numbers. For example, *TgBAC(pdgfrb:EGFP)*^{ncv22} is abbreviated to *TgBAC(pdgfrb:EGFP)*.

FACS and RT-PCR

Cranial parts of 60 *TgBAC(pdgfrb:EGFP);Tg(fli:Myr-mCherry)* larvae at 7 dpf were cut out and dissociated in 2 ml of protease solution (1% trypsin, 1 mM EDTA, pH 8.0 in PBS) containing 2.7 mg/ml collagenase P (Roche, Mannheim, Germany) for 1 h with gently pipetting every 30 min. The reaction was terminated by addition of 200 µl of stop solution (30% fetal bovine serum, 6 mM $CaCl_2$ in PBS). The dissociated cells were pelleted by centrifugation at 3,000 rpm for 5 min at 4 °C and washed with 1 ml ice-cold suspension media (1% fetal bovine serum, 0.8 mM $CaCl_2$, 50 U/ml penicillin, 0.05 mg/ml streptomycin in phenol red free DMEM [GIBCO, Grand Island, NY]). After the centrifugation, the cells were resuspended in 1 ml of ice-cold suspension media and sorted using a FACS Aria III sorter (BD Bioscience, San Jose, CA). The sorted cells

were then grouped into EGFP-negative/mCherry negative (double negative), EGFP-positive/mCherry negative (pdgfrb:EGFP (+), fli1a:Myr-mCherry (-)) and EGFP-negative/mCherry-positive (pdgfrb:EGFP (-), fli1a:Myr-mCherry (+)) cell populations. Total RNAs were purified from the sorted cells by using NucleoSpin RNA XS kit (Macherey-Nagel, Düren, Germany) and reverse transcribed by random hexamer primers using Superscript III (Invitrogen) according to the manufacturers' instructions. PCR amplification was carried out using KOD-FX (TOYOBO, Osaka, Japan) and the following primer sets: *pdgfrb*, 5'- CGTTCCCAGGAGCCTTTTCT-3' and 5'- TTGGGATCAGGGATGGGGAT-3'; *cspg4*, 5'-AAGTGGCAAGATGAGAGCCC-3' and 5'- ATGCTCCATTGGTGGTCTGG-3'; *acta2*, 5'- CCCAGCACTGTCAGGTGATT-3' and 5'- AAGCCTGCCTTACACAGTCC-3'; *tie1*, 5'- CATGGAGATCGCTGTCGTAA-3' and 5'- TGCATTTGCCTTTGTTCTTG-3'; *tie2*, 5'- AGCACACTCTCCTCACAGCA-3' and 5'- TTCGCCACAAAGTTCTCTCC-3'; *ef1a1l1* (*ef1a*), 5'- TCACCCTGGGAGTGAAACAGC-3' and 5'- ACTTGCAGGCGATGTGAGCAG-3'.

Immunohistochemistry

Approximately 1 mpf *TgBAC(pdgfrb:EGFP);Tg(fli1a:Myr-mCherry)* and *TgBAC(tagln:EGFP);Tg(fli1a:Myr-mCherry)* zebrafish were anesthetized and fixed with 4% paraformaldehyde at 4 °C overnight. After washing with PBS, their skins and scales were removed using scissors and forceps. The pleura region as shown in Fig. 1H and the caudal region as depicted in Fig. S1H were embedded in 4% agarose and cut transversely with VT1200S vibratome (Leica Microsystems, Wetzlar, Germany) into 200 µm sections. The tissue sections were washed with PBS-Tween 20 (PBST)

containing 0.1% TritonX-100 three times every for 5 min at 4 °C with shaking and treated with blocking reagent (5% sheep serum, 1% BSA and 0.1% TritonX-100 in PBST) for 1 h at R.T. Then, the samples were immunostained with anti-α-SMA antibody (sc-53142) (Santa Cruz Biotechnology, Inc., Santa Cruz, CA) at 4°C overnight. Protein reacting with primary antibody was visualized with Alexa Fluor 633-labeled anti-mouse IgG (Molecular Probes, Invitrogen, Eugene, OR). Fluorescence images were obtained using a FluoView FV1000 or FV1200 confocal upright microscope (Olympus) equipped with water-immersion 20x (XLUMPlanFL, 1.0 NA) lens.

Injections of morpholino oligonucleotides

Control morpholino oligonucleotide (MO) (Gene Tools, LLC, Philomath, OR), 2 ng of *tnnt2a* MO, 4 ng of *foxd3* MO, 4 ng of *tfap2a* MO, 5 ng of *tbx6* MO or 5 ng of *hand2* MO was injected into embryos at one-cell stage. The sequence for the already-validated MOs used in this study are: *tnnt2a* MO, 5'-CATGTTTGCTCTGATCTGACACGCA-3' (Sehnert et al., 2002); *foxd3* MO, 5'- TGCTGCTGGAGCAACCCAAGGTAAG-3' (Whitesell et al., 2014); *tfap2a* MO, 5'- CCTCCATTCTTAGATTTGGCCCTAT-3' (Whitesell et al., 2014); *tbx6* MO, 5'- CATTTCCACACCCAGCATGTCTCGG-3' (Kawamura et al., 2005); *hand2* MO, 5'- CCTCCAACTAAACTCATGGCGACAG-3' (Reichenbach et al., 2008).

Supplemental Figures

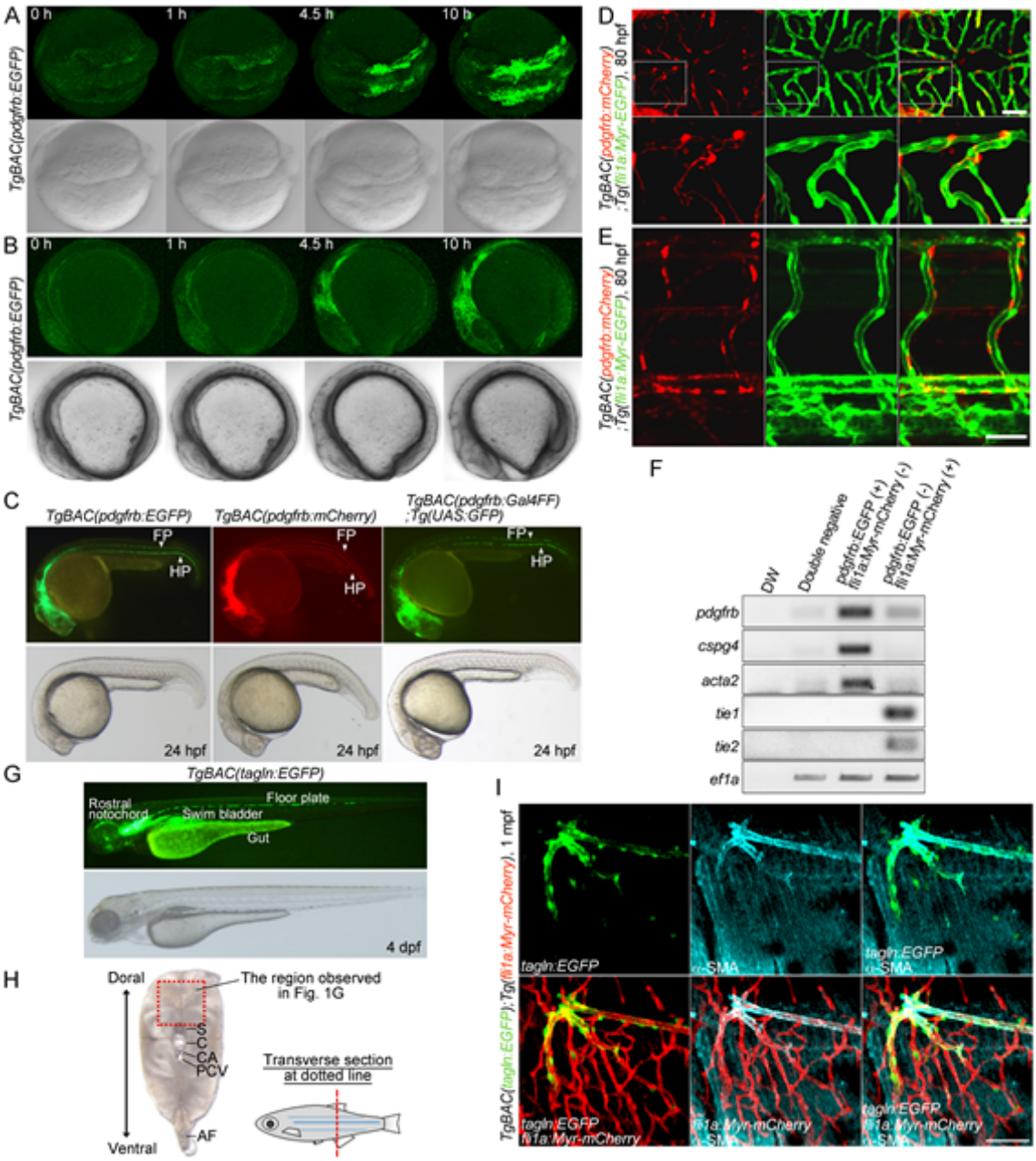

Figure S1. Characterization of *TgBAC(pdgfrb:EGFP)* and *TgBAC(tagln:EGFP)* zebrafish lines. (**A**, **B**) Time-lapse confocal images of the *TgBAC(pdgfrb:EGFP)* embryos from 8 somite stage. Dorsal (**A**) and lateral (**B**) view images at 8 somite stage (leftmost column) and their subsequent time-lapse images with the elapsed time (h) at the top. Upper, *pdgfrb:EGFP*; lower, bright field image. (**C**) Lateral views of *TgBAC(pdgfrb:EGFP)* (left), *TgBAC(pdgfrb:mCherry)* (center) and *TgBAC(pdgfrb:Gal4FF);Tg(UAS:GFP)* (right) zebrafish embryos at 24 hpf. Upper, *pdgfrb:EGFP* (left), *pdgfrb:mCherry* (center) and *pdgfrb:Gal4FF;UAS:GFP* (right);

lower, bright field images. FP, floor plate; HP, hypochord. (**D**, **E**) Dorsal view of CtAs (**D**) and lateral view of trunk vessels (**E**) in the *TgBAC(pdgfrb:mCherry);Tg(fli1a:Myr-EGFP)* larvae at 80 hpf. Anterior to the left. Left; *pdgfrb:mCherry*, center; *fli1a:Myr-EGFP*, right; the merged images of *pdgfrb:mCherry* (red) and *fli1a:Myr-EGFP* (green). The boxed areas in **D** are enlarged at the bottom. (**F**) Expression of MC markers (*pdgfrb*, *cspg4*, and *acta2*), EC markers (*tie1* and *tie2*) and *ef1a* in the EGFF and mCherry double-negative cells (Double negative), EGFP-positive and mCherry-negative cells (pdgfrb:EGFP (+), fli1a:Myr-mCherry (-)) and EGFP-negative and mCherry-positive cells (pdgfrb:EGFP (-), fli1a:Myr-mCherry (+)) isolated from the *TgBAC(pdgfrb:EGFP);Tg(fli:Myr-mCherry)* larvae by FACS at 7 dpf was analyzed by RT-PCR analyses. (**G**) Lateral view of the *TgBAC(tagln:EGFP)* zebrafish larva at 4 dpf. Upper, *tagln:EGFP*; lower, bright field image. (**H**) Transverse sectional image of caudal region of adult zebrafish. The boxed area indicates the region where the images shown in Figure **1G** were taken. S, spinal cord; C, caudal vertebra; CA, caudal artery; PCV, posterior cardinal vein; AF, anal fin. (**I**) Confocal images of blood vessels in the intercostal muscle of the 1 mpf *TgBAC(tagln:EGFP);Tg(fli1a:Myr-mCherry)* juvenile. The pleural tissue was immunostained with anti-α-SMA antibody to visualize VSMC, as in Fig. **1H**. *tagln:EGFP* (green), α-SMA (blue) and *fli1a:Myr-mCherry* (red) images are shown as indicated at the bottom left corner of each image. Scale bars, 20 μm (enlarged image in **D**), 50 μm (**D**, **E**, **I**).

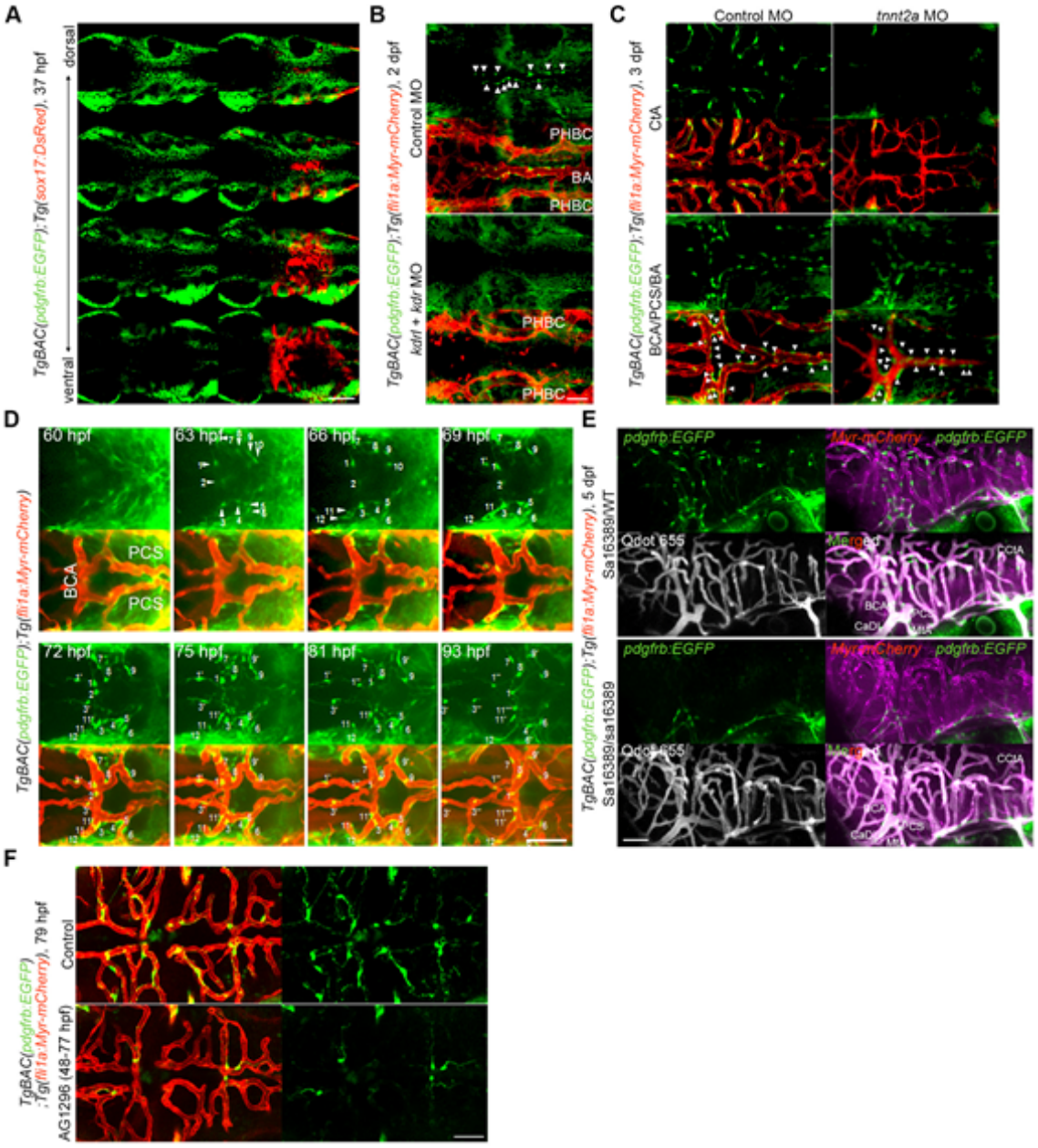

Figure S2. MC coverage of cranial vessels. (**A**) Confocal images of cranial region in the *TgBAC(pdgfrb:EGFP);Tg(sox17:DsRed)* embryo at 37 hpf. Dorsal view, anterior to the left. Multiple single z-plane images are shown (from the top (dorsal) to the bottom (ventral)). Left, *pdgfrb:EGFP*; right, the merged images of *pdgfrb:EGFP* (green) and *sox17:DsRed* (red). Note that EGFP-positive cells were not identical to DsRed-positive endodermal cells. (**B**) Confocal images of hindbrain vasculature in the 2 dpf *TgBAC(pdgfrb:EGFP);Tg(fli1a:Myr-mCherry)* embryos injected with control MO (upper two panels) or both *kdrl* and *kdr* MOs (lower two panels). Upper, *pdgfrb:EGFP*; lower, the merged images of *pdgfrb:EGFP* (green) and *fli1a:Myr-mCherry* (red).

Arrowheads indicate the MCs covering the BA. Note that *kdrl*/*kdr*-double morphant exhibited not only defective formation of BA but also lack of MCs in the midline of the cerebral base. (**C**) Confocal images of CtA (upper tow panels) and the vessels in the cerebral base (BCA/PCS/BA, lower two panels) in the 3 dpf *TgBAC(pdgfrb:EGFP);Tg(fli1a:Myr-mCherry)* larvae injected with control MO (left column) or *tnnt2a* MO (right column). Upper, *pdgfrb:EGFP*; lower, the merged images of *pdgfrb:EGFP* (green) and *fli1a:Myr-mCherry* (red). Arrowheads indicate the MCs covering the BCA, PCS and BA. Note that MC coverage was observed in the vessels in the cerebral base but not in the CtA of *tnn2a* morphants. (**D**) Time-lapse confocal images of the cranial vasculature in the *TgBAC(pdgfrb:EGFP);Tg(fli1a:Myr-mCherry)* embryo (60-93 hpf). Dorsal view, anterior to the left. Upper, *pdgfrb:EGFP*; lower, the merged images of *pdgfrb:EGFP* (green) and *fli1a:Myr-mCherry* (red). Numbers indicate individual EGFP-positive cells emerging around the PCS and BCA. EGFP-positive cells designated with prime marks indicate progeny cells. (**E**) Confocal images of cranial vessels of *pdgfrb* heterozygous (upper two panels, sa16389/WT) and homozygous (lower two panels, sa16389/sa16389) larvae in the *TgBAC(pdgfrb:EGFP);Tg(fli1a:Myr-mCherry)* background at 5 dpf. Lateral view, anterior to the left. To assess blood flow and blood vessel lumenization, Qdot 655 fluorescent probe was injected into the common cardinal vein just before imaging. Upper left, *pdgfrb:EGFP*; lower left, Qdot 655; upper right, the merged images of *pdgfrb:EGFP* (green) and *fli1a:Myr-mCherry* (magenta); lower right, the merged images of *pdgfrb:EGFP* (green), *fli1a:Myr-mCherry* (magenta) and Qdot 655 (white). (**F**) Confocal images of CtA in the *TgBAC(pdgfrb:EGFP);Tg(fli1a:Myr-mCherry)* larva treated with vehicle (upper) or 20 μM AG1296 (lower) during 48-77 hpf. Dorsal view, anterior to the left. Left, the merged images of *pdgfrb:EGFP* (green) and *fli1a:Myr-mCherry* (red); right, *pdgfrb:EGFP*. BA, basilar artery; PHBC, primordial hindbrain channel; CCtA, cerebellar central artery; BCA, basal communicating artery; PCS, posterior communicating segment; CaDI, caudal division of the internal carotid artery; MtA, metencephalic artery. Scale bars, 50 μm.

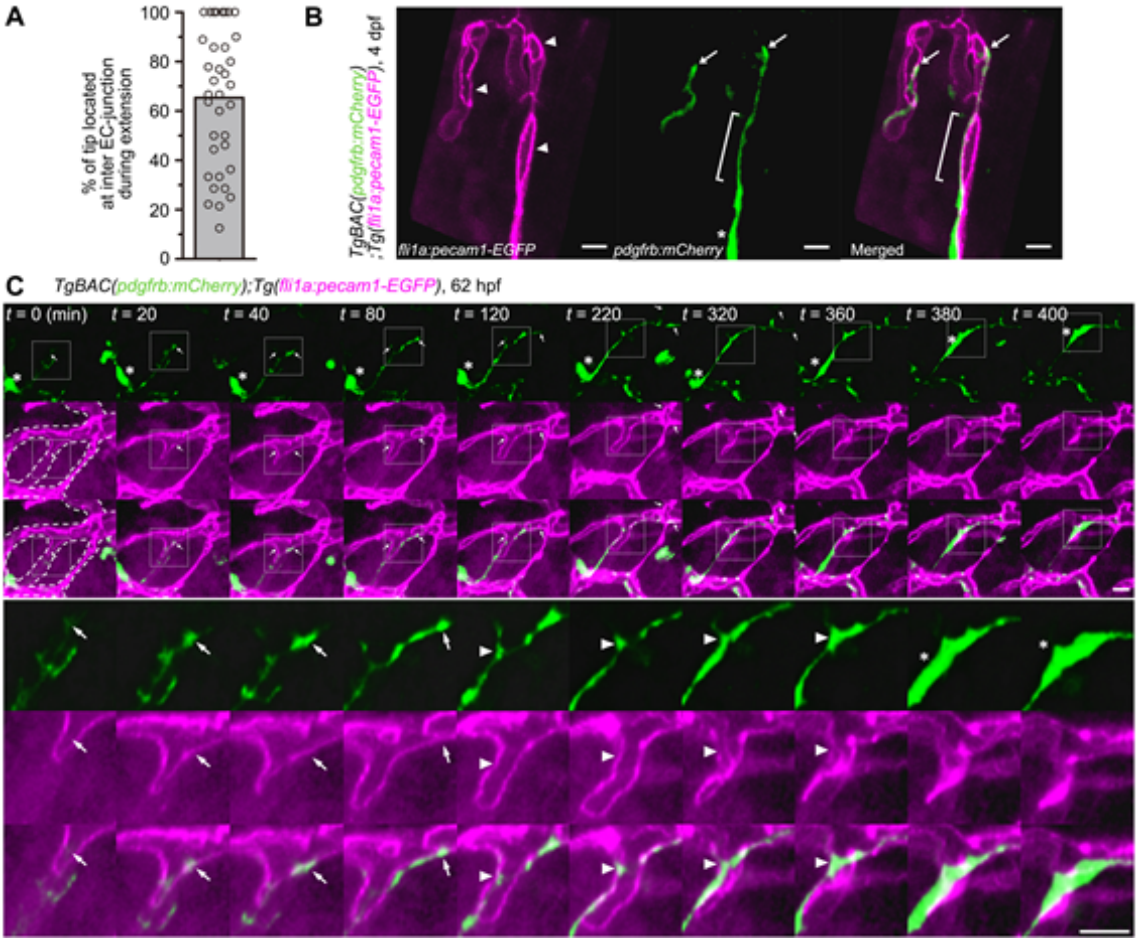

Figure S3. Extension of MC processes and MC migration along the inter-EC junctions. (**A**) Frequency of tip location of MC processes at the inter-EC junctions during their extension. By time-lapse imaging the *TgBAC(pdgfrb:mCherry);Tg(fli1a:pecam1-EGFP)* larvae as observed in Fig. **3A**, tip location of the MC process was examined every 15 or 20 min for more than 1 h. Data are expressed as a percentage of number of time points at which the tip of MC process located at the inter-EC junction among the total time points. Bar and circles indicate the average and the values of each process, respectively (n=36). (**B**) Confocal images of the MCs and inter-EC junctions in the CtA of the 4 dpf *TgBAC(pdgfrb:mCherry);Tg(fli1a:pecam1-EGFP)* larva. Left, *fli1a:pecam1-EGFP*; center, *pdgfrb:mCherry*; right, the merged image of *fli1a:pecam1-EGFP* (magenta) and *pdgfrb:mCherry* (green). Arrowheads indicate the inter-EC junctions visualized by Pecam1-EGFP, while arrows show the tip of MC processes. Brackets indicate the MC process aligned along the inter-EC junction. Asterisk indicates cell body of MC. The cell body of the MC shown in the left side of the image is out of frame. Scale bar, 10 µm. (**C**) Time-lapse confocal images of MC migration along the CtA in the hindbrain of the

TgBAC(pdgfrb:mCherry);Tg(fli1a:pecam1-EGFP) larva. 3D-rendered confocal images and its subsequent time-lapse images with the elapsed time (min) at the top are shown, as in Fig. **3A**. The boxed areas are enlarged beneath the original images. Dotted-lines in second and third rows of the leftmost column outline the vessel morphology. Arrows indicate the tip of MC process, while asterisks show the cell body. Note that the tip of MC process moved forward along the inter-EC junction and that the MC-body (asterisks) was relocated to the preceding process which aligned along the inter-EC junctions (arrowheads). Scale bars, 10 μm.

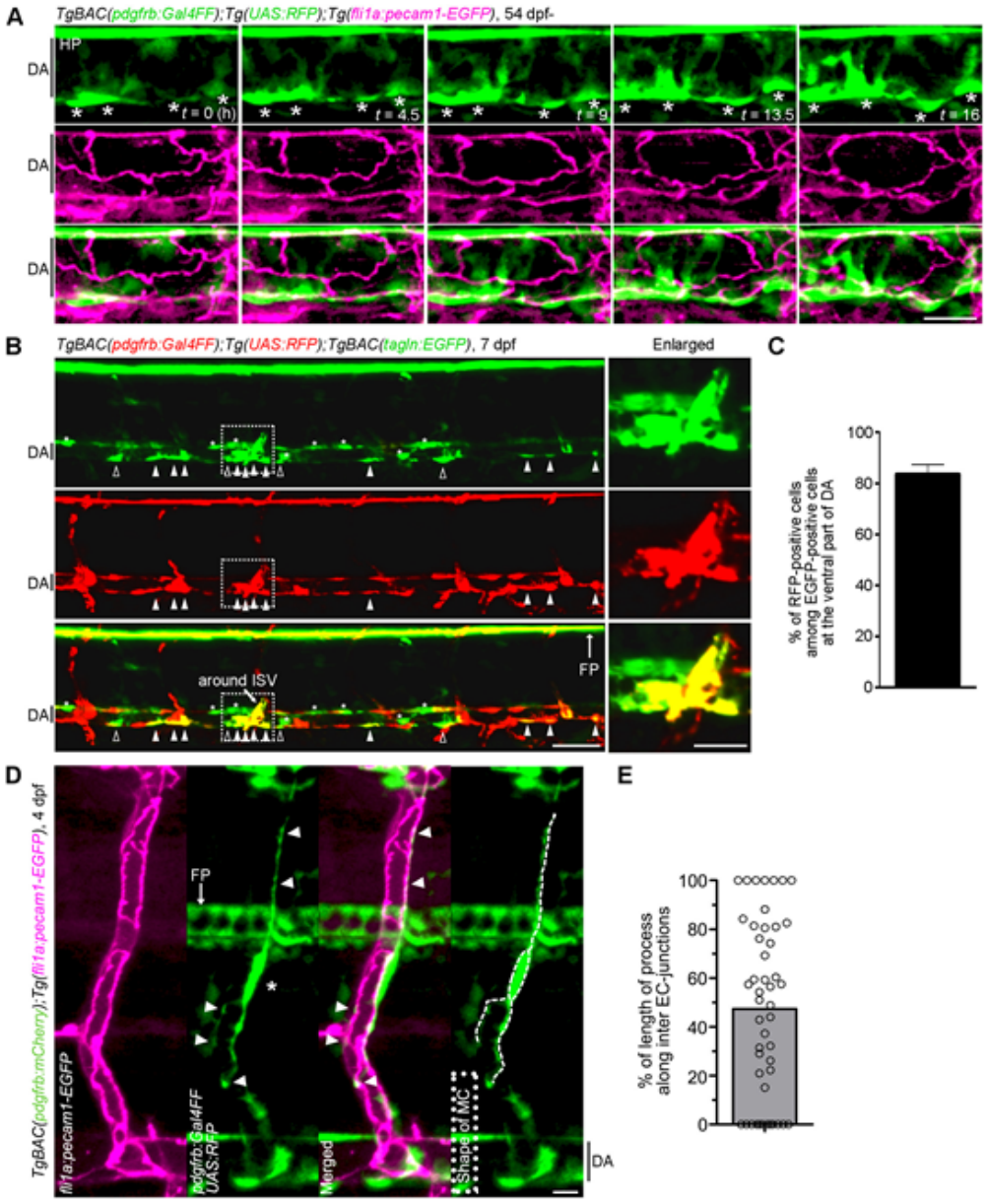

Figure S4. MC coverage of trunk axial vessels. (**A**) Time-lapse confocal images of MC coverage of DA. Confocal images of DA in the *TgBAC(pdgfrb:Gal4FF);Tg(UAS:RFP);Tg(fli1a:pecam1-EGFP)* embryo at 54 hpf (leftmost column) and subsequent time-lapse images with the elapsed time (h) at the bottom right. Top, *pdgfr:Gal4FF;UAS:RFP* (green); middle, *fli1a:pecam1-EGFP* (magenta); bottom, the merged images of *pdgfr:Gal4FF;UAS:RFP* (green) and *fli1a:pecam1-EGFP* (magenta). Asterisks indicate the cell body of MCs. Note that MCs located at the ventral side of DA extended multiple processes dorsally irrespective of inter EC-junctions. (**B**) Confocal images of trunk vasculature in the *TgBAC(pdgfrb:Gal4FF);Tg(UAS:RFP);TgBAC(tagln:EGFP)* larva at 7 dpf. Top,

tagln:EGFP; meddle, *pdgfr:Gal4FF;UAS:RFP*; lower, the merged image of *tagln:EGFP* (green) and *pdgfr:Gal4FF;UAS:RFP* (red). The boxed areas are enlarged to the right. Open and closed triangles indicate the EGFP-positive and RFP-positive cells and the EGFP-positive and RFP-negative cells at the ventral side of the DA, respectively. Asterisks indicate the EGFP-positive and RFP-negative cells located in the dorsal and lateral side of the DA. (**C**) Percentage of RFP-positive cells among the EGFP-positive cells located at the ventral side of the DA, as observed in **B**. Data is mean ± s.e.m. (n = 15). (**D**) Confocal images of an ISV in the *TgBAC(pdgfrb:mCherry);Tg(fli1a:pecam1-EGFP)* larva at 4 dpf. Lateral view, anterior to the left. Leftmost panel, *fli1a:pecam1-EGFP* (magenta); second panel from the left, *pdgfr:Gal4FF;UAS:RFP* (green); third panel from the left, the merged image of *fli1a:pecam1-EGFP* image (magenta) and *pdgfr:Gal4FF;UAS:RFP* (green); rightmost panel, *pdgfr:Gal4FF;UAS:RFP* image in which MC shape is outlined by the dotted line. Arrowheads indicate the MC processes that aligned along with Pecam1-EGFP-labeled inter-EC junctions. Asterisk shows the MC body. (**E**) Alignment of MC processes along the inter-EC junctions as observed in **D** is expressed as a percentage of the total length (n = 47). Bar and circles indicate the average and the values of individual process, respectively. In this figure, all images are shown in lateral view with anterior to the left. Scale bars; 20 μm (**D**, enlarged image in **B**) or 50 μm (**A**, **B**). DA, dorsal aorta; HP, hypochord; FP, floor plate.

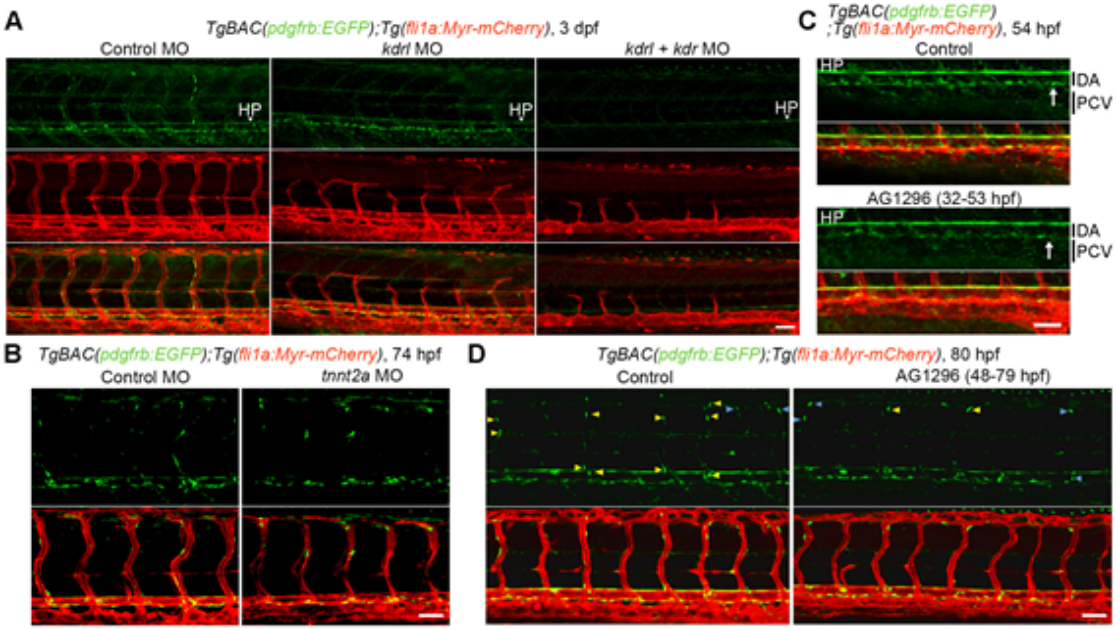

Figure S5. Developmental mechanism of MCs in the trunk vasculature. (**A**) Confocal images of trunk vasculature in the 3 dpf *TgBAC(pdgfrb:EGFP);Tg(fli1a:Myr-mCherry)* larvae injected with control MO (left), *kdrl* MO (center) or both *kdrl* and *kdr* MOs (right). Top, *pdgfrb:EGFP*; middle, *fli1a:Myr-mCherry* (red); bottom, the merged images of *pdgfrb:EGFP* (green) and *fli1a:Myr-mCherry* (red). (**B**) Confocal images of trunk vasculature in the 3 dpf *TgBAC(pdgfrb:EGFP);Tg(fli1a:Myr-mCherry)* embryo injected with control MO (left) or *tnnt2a* MO (right). Upper, *pdgfrb:EGFP*; lower, the merged images of *pdgfrb:EGFP* (green) and *fli1a:Myr-mCherry* (red). (**C**, **D**) Confocal images of trunk vasculature in the 54 hpf (**C**) or 80 hpf (**D**) *TgBAC(pdgfrb:EGFP);Tg(fli1a:Myr-mCherry)* larvae treated with vehicle or 20 μM AG1296 during 32-53 hpf (**C**) or 48-79 hpf (**D**). Upper, *pdgfrb:EGFP*; lower, the merged images of *pdgfrb:EGFP* (green) and *fli1a:Myr-mCherry* (red). Arrows in **C** indicate the EGFP-positive cells beneath the DA. Yellow and blue arrowheads in **D** indicate the EGFP-positive cells covering aISVs and those covering vISVs, respectively. In this figure, all images are shown in lateral view with anterior to the left. Scale bars, 20 μm (enlarged image in **A**) or 50 μm (**A**-**D**). DA, dorsal aorta; PCV, posterior cardinal vein; HP, hypochord.

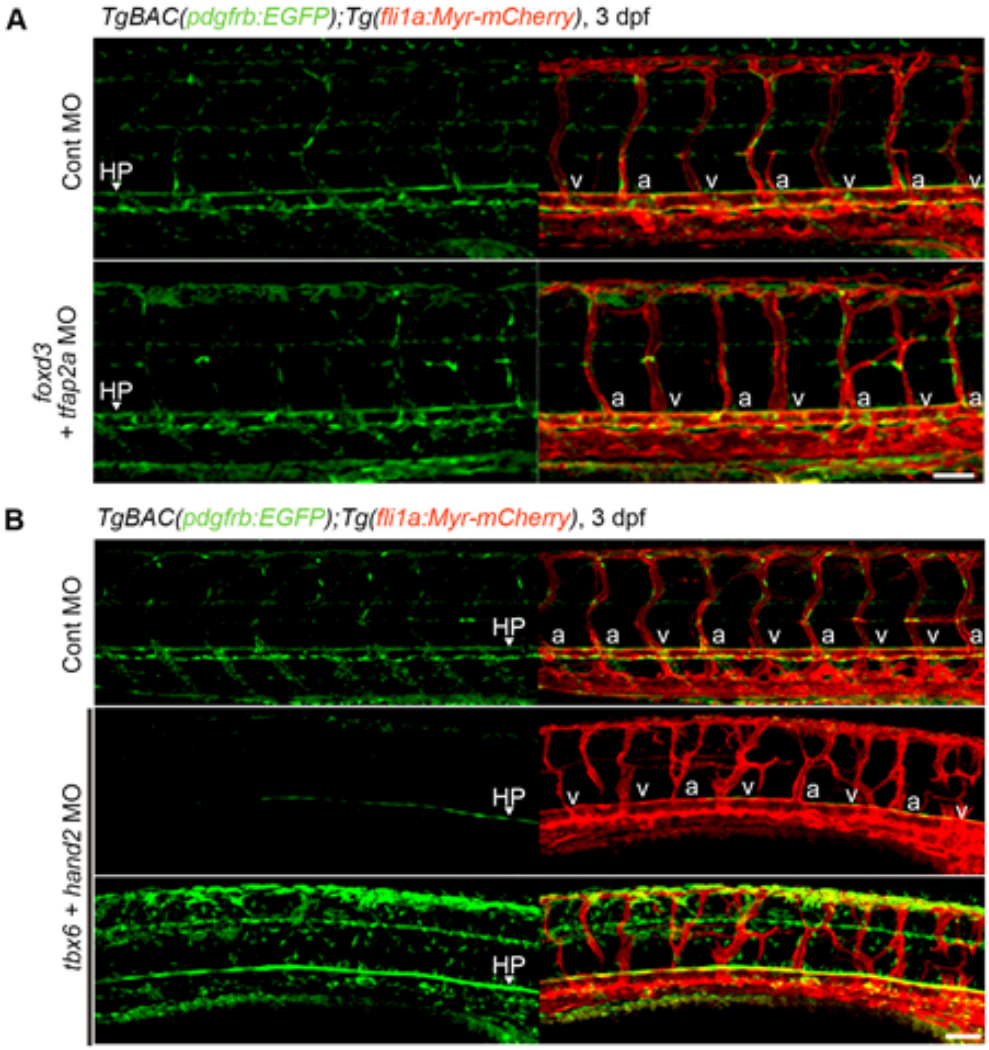

Figure S6. Investigation of the origin of the MCs in trunk vessels. (**A**) Confocal images of trunk vasculature in the 3 dpf *TgBAC(pdgfrb:EGFP);Tg(fli1a:Myr-mCherry)* larvae injected with control MO (upper) or both *foxd3* and *tfap2a* MOs (lower). Left, *pdgfrb:EGFP*; right, the merged images of *pdgfrb:EGFP* (green) and *fli1a:Myr-mCherry* (red). (**B**) Confocal images of trunk vasculature in the 3 dpf *TgBAC(pdgfrb:EGFP);Tg(fli1a:Myr-mCherry)* larvae injected with control MO (top) or both *tbx6* and *hand2* MOs (middle and bottom). Left, *pdgfrb:EGFP*; right, the merged images of *pdgfrb:EGFP* (green) and *fli1a:Myr-mCherry* (red). In the bottom panel, GFP signal is intensified to detect the weak signal. HP, hypochord. "a" and "v" indicate arterial ISVs (aISV) and venous ISVs (vISV), respectively. Scale bars, 50 μm.

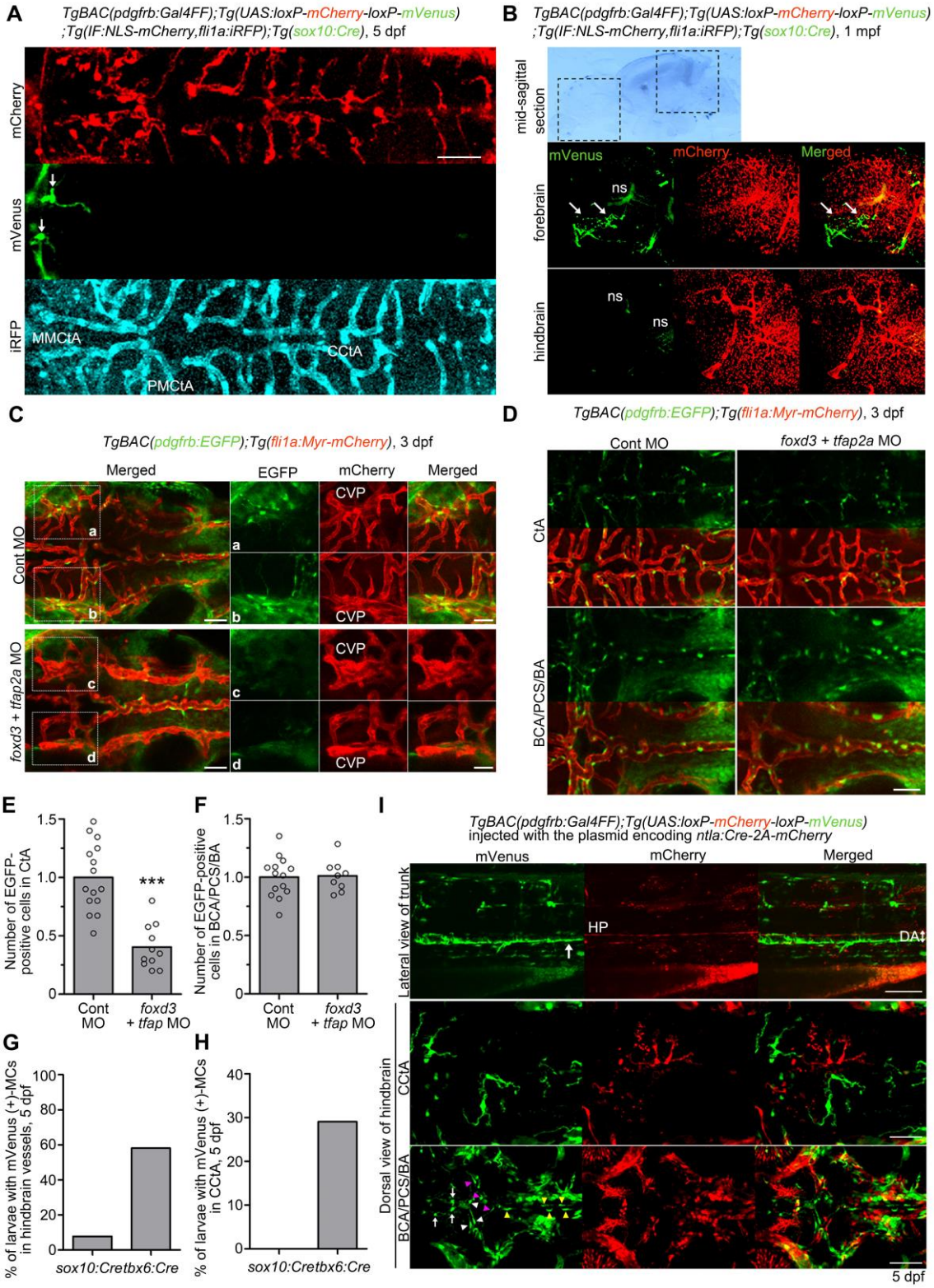

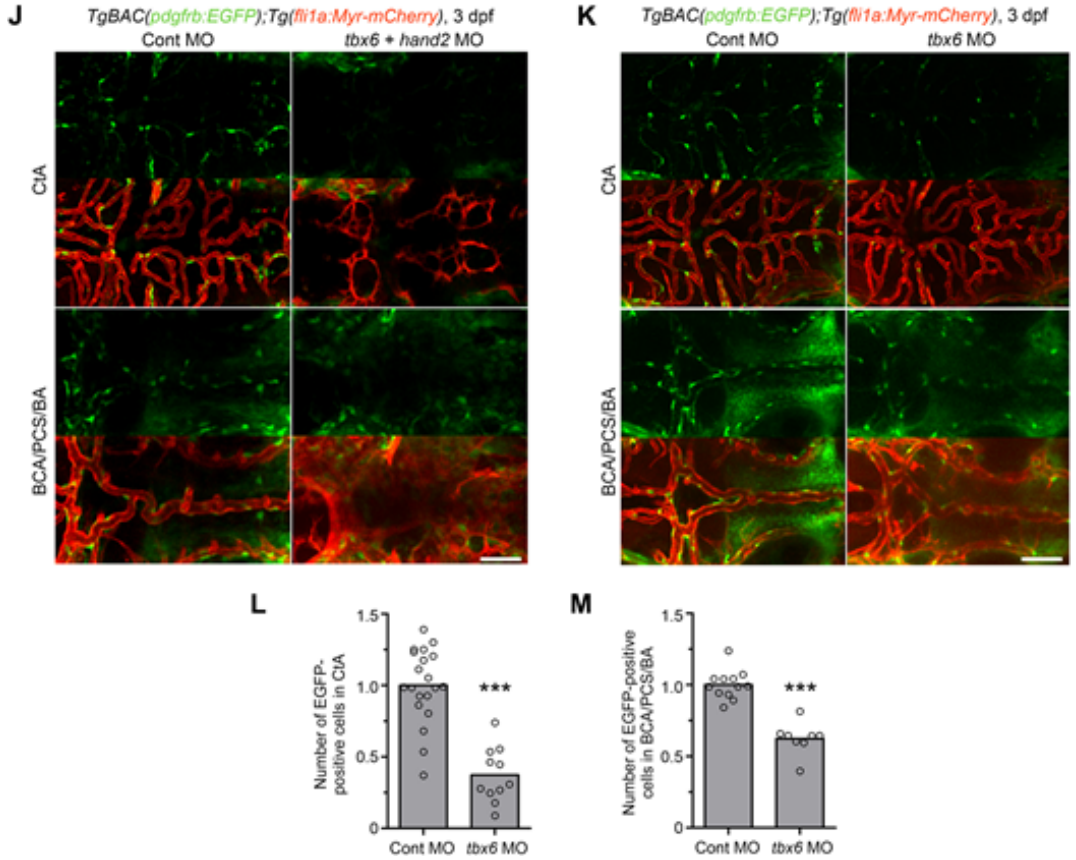

Figure S7. Investigation of the origin of the MCs in cranial vessels. (**A**) Confocal images of CtA in the *TgBAC(pdgfrb:Gal4FF);Tg(UAS:loxP-mCherry-loxP-mVenus);Tg(IF:NLS-mCherry,fli1a:iRFP);Tg(sox10:Cre)* larva at 5 dpf. The larvae expressing iRFP670 under the control of *fli1a* promoter was identified by *intestinal fatty acid binding protein* (*IF*) promoter-driven expression of NLS-mCherry in the intestine. Dorsal view, anterior to the left. Top, mCherry; middle, mVenus; bottom, iRFP. Arrows indicate mVenus-positive MCs. Note that the mVenus-positive MCs existed in anterior part of MMCtA, but not in the PMCtA and CCtA, at 5 dpf. (**B**) Midsagittal section of brain of the *TgBAC(pdgfrb:Gal4FF):Tg(UAS:loxP-mCherry-loxP-mVenus);Tg(IF:NLS-mCherry,fli1a:iRFP);Tg(sox10:Cre)* juvenile at 1 mpf. Confocal images of forebrain (middle panel) and hindbrain (bottom panel) indicated by the boxed areas in the bright field image (upper panel). Left, mVenus; center, mCherry; right, the merged images of mVenus (green) and mCherry (red). Arrows indicate mVenus-positive MCs. Note that the mVenus-positive MCs existed in the forebrain, but not in the hindbrain, at 1 mpf. ns indicates non-specific intrinsic fluorescence signal. (**C**) Confocal images of the vessels in the cerebral base in the 3 dpf *TgBAC(pdgfrb:EGFP);Tg(fli1:Myr-mCherry)* larvae

injected with control MO (upper panels) or both *foxd3* and *tfap2a* MOs (lower panels). Dorsal view, anterior to the left. The merged images of *pdgfrb:EGFP* (green) and *fli1a:Myr-mCherry* (red) are shown at the leftmost column. Boxed areas (**a-d**) are enlarged to the right, showing *pdgfrb:EGFP* (left), *fli1a:Myr-mCherry* (center) and the merged images of *pdgfrb:EGFP* (green) and *fli1a:Myr-mCherry* (red) (right). Note that *pdgfrb:EGFP*-positive cells around CVP were dramatically reduced in the *foxd3*/*tfap2a*-double morphant larvae. (**D**) Confocal images of CtA (upper two panel) and the vessels in the cerebral base (lower two panels, BCA/PCS/BA) in the 3 dpf *TgBAC(pdgfrb:EGFP);Tg(fli1a:Myr-mCherry)* larvae injected with control MO (left column) or both *foxd3* and *tfap2a* MOs (right column). Dorsal view, anterior to the left. Upper, *pdgfrb:EGFP*; lower, the merged images of *pdgfrb:EGFP* (green) and *fli1a:Myr-mCherry* (red). (**E**, **F**) The number of EGFP-positive cells covering the CtA (**E**) or the BCA, PCS and BA (**F**), as observed in **D**. Data are expressed relative to the average of controls ($n \geq 9$). (**G**, **H**) Percentage of larvae showing mVenus-positive MCs covering the vessels in the hindbrain such as CCtA, BCA, PCS and BA (**G**) or in the CCtA (**H**) of the 5 dpf *TgBAC(pdgfrb:Gal4FF):Tg(UAS:loxP-mCherry-loxP-mVenus)* larvae crossed with *Tg(sox10:Cre)* (sox10:Cre) or *Tg(tbx6:Cre,myl7:EGFP)* (tbx6:Cre) fish line (sox10:Cre n=13, tbx6:Cre n=31). (**I**) Confocal images of trunk (upper panel; lateral view, anterior to the left) and head (middle (CCtA) and lower (BCA, PCS, and BA) panels; dorsal view, anterior to the left) regions in the 5 dpf *TgBAC(pdgfrb:Gal4FF):Tg(UAS:loxP-mCherry-loxP-mVenus)* larvae injected with the plasmid encoding *ntla:Cre-2A-mCherry*. Note that mVenus-positive MCs covered the ventral part of DA (arrow) in the trunk and the CCtA, BCA (white arrowheads), PCS (magenta arrowheads), BA (yellow arrowheads) and PMCtA (arrows) in the head. HP; hypochord. (**J**) Confocal images of the CtA (upper two panels) and the vessels in the cerebral base (BCA/PCS/BA, lower two panels) in the 3 dpf *TgBAC(pdgfrb:EGFP);Tg(fli1a:Myr-mCherry)* larvae injected with control MO (left column) or both *tbx6* and *hand2* MOs (right column). Upper, *pdgfrb:EGFP*; lower, the merged images of *pdgfrb:EGFP* (green) and *fli1a:Myr-mCherry* (red). Note that *tbx6/hand2*-double morphant exhibited defective formation of hindbrain vessels. (**K**) Confocal images of the CtA and the vessels in the cerebral base in the 3 dpf *TgBAC(pdgfrb:EGFP);Tg(fli1a:Myr-mCherry)* larvae injected with control MO (left column) or *tbx6* MO (right column) are shown, as in **J**. (**L**, **M**) The number of EGFP-positive cells covering the CtA (**L**) or the BCA, PCS and BA (**M**), as observed in **K**. Data are expressed relative to the average of controls ($n \geq 8$). Bars and circles indicate averages and each value, respectively. Scale bars, 20 μm (enlarged images in

C) or 50 μm (**A-D**, **I-K**). In **E**, **F**, **L** and **M**, bars and circles indicate averages and each value, respectively. In **E**, **L** and **M**, ***p<0.001, significant difference between two groups.

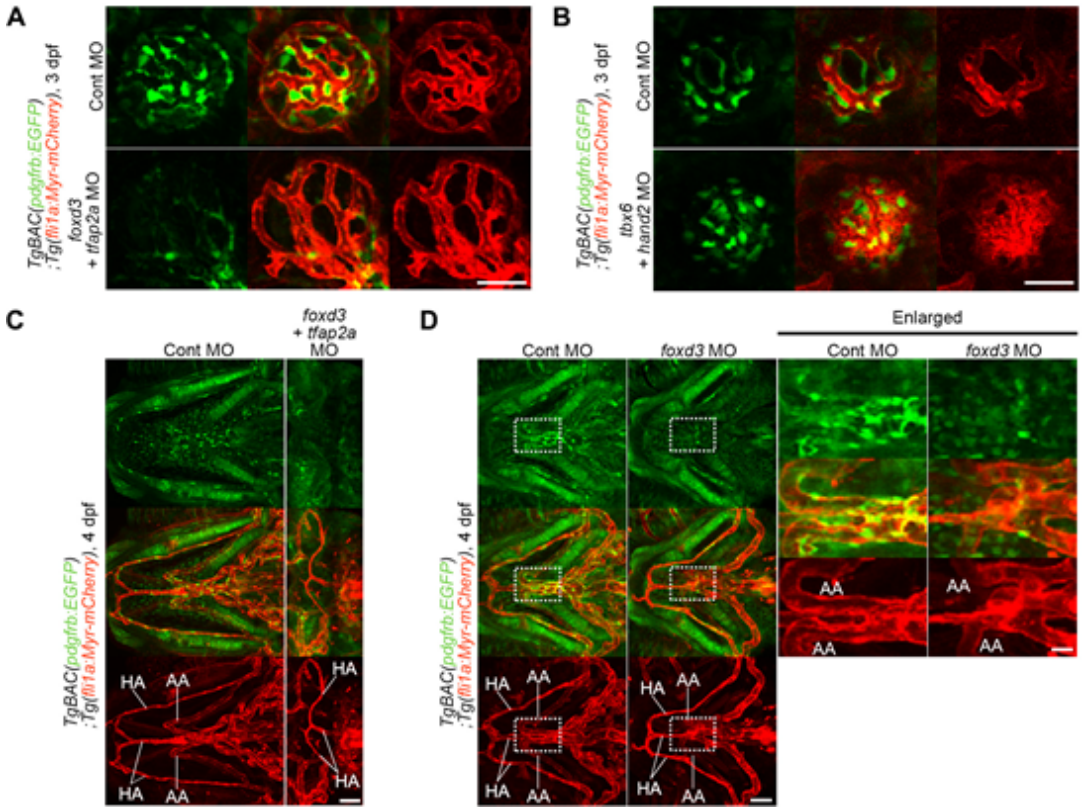

Figure S8 Investigation of the origin of MCs in the hyaloid vessels and the vessels in the pharyngeal region. (**A**) Confocal images of hyaloid vessels in the 3 dpf *TgBAC(pdgfrb:EGFP);Tg(fli1a:Myr-mCherry)* larvae injected with control MO (upper panels in **A** and **B**) or either both *foxd3* and *tfap2a* MOs (lower panel in **A**) or both *tbx6* and *hand2* MOs (lower panel in **B**). Lateral view, anterior to the left. Left, *pdgfrb:EGFP*; center, the merged images of *pdgfrb:EGFP* (green) and *fli1a:Myr-mCherry* (red); right, *fli1a:Myr-mCherry*. (**C**, **D**) Confocal images of vessels in the pharyngeal region in the 4 dpf *TgBAC(pdgfrb:EGFP);Tg(fli1a:Myr-mCherry)* larvae injected with control MO (left columns in **C** and **D**) or either both *foxd3* and *tfap2a* MOs (right column in **C**) or *foxd3* MO (right column in **D**). Top, *pdgfrb:EGFP*; middle, the merged images of *pdgfrb:EGFP* (green) and *fli1a:Myr-mCherry* (red); bottom, *fli1a:Myr-mCherry*. In **D**, the boxed areas are enlarged to the right. Note that *foxd3*/*tfap2a*-double morphant larva exhibited severe structural defects in the head, although it could form abnormal HA. AA, aortic arches; HA, hypobranchial artery. Scale bars, 20 μm (enlarged image in **D**) or 50 μm (**A**-**E**).

Movies

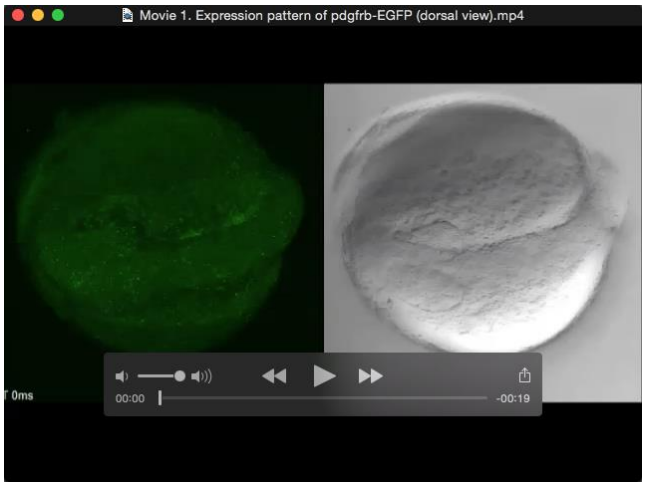

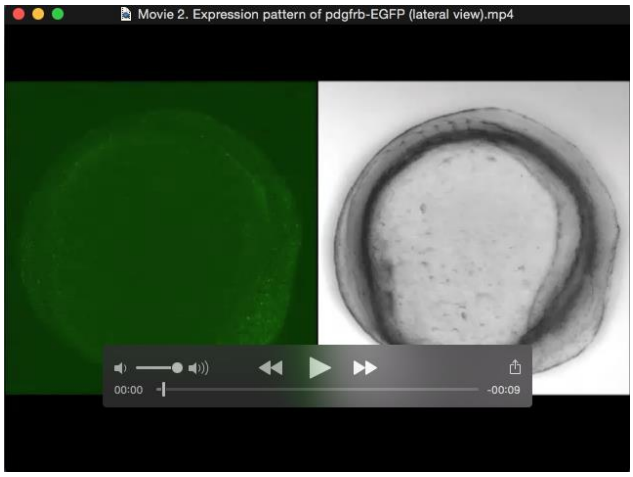

Movie 1 and 2. Expression pattern of EGFP in the early stage of *TgBAC(pdgfrb:EGFP)* embryos.
Time-lapse confocal imaging of EGFP fluorescence in the *TgBAC(pdgfrb:EGFP)* embryos from 8 somite stage. Images were obtained every 45 min. In movie 1, anterior to the left (dorsal view). In movie 2, anterior to the right (lateral view).

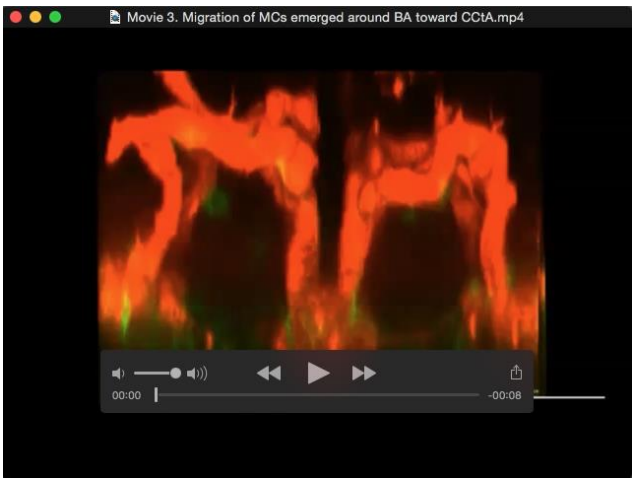

Movie 3. Migration of MCs emerged around BA along the CCtA.
Time-lapse confocal imaging of MC coverage of CCtAs in the *TgBAC(pdgfrb:EGFP);Tg(fli1a:Myr-mCherry)* larva (57-71 hpf). Lateral view, dorsal to the top and anterior to the front. Green, EGFP fluorescence; red, mCherry fluorescence. Note that EGFP-positive cells located around the BA dorsally migrated along the CCtA.

Movie 4 and 5. Dynamics of MCs during their migration along the CtA.
Time-lapse confocal imaging of cranial vasculature in the *TgBAC(pdgfrb:EGFP);Tg(fli1a:Myr-mCherry)* larva (57-88 hpf). Dorsal view, anterior to the left. Movie 4, merged image of EGFP (green) and mCherry (red); movie 5, EGFP image. Note that EGFP-positive cells covering the vessels located in the cerebral base such as BA, BCA, PCS and CVP migrated toward the CtAs that include CCtA, PMCtA, AMCtA and MMCtA.

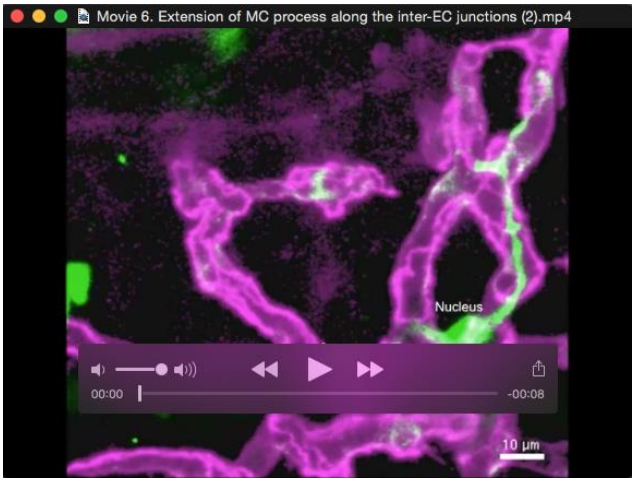

Movie 6. Extension of MC process along the inter-EC junctions.
Time-lapse confocal imaging of CtA in the *TgBAC(pdgfrb:mCherry);Tg(fli1a:pecam1-EGFP)* larva starting from 62 hpf, as shown in Fig 3A. Images were obtained every 15 min. Green, mCherry (MC); Magenta, EGFP (Pecam1-EGFP-labeled inter-EC junctions). Arrowhead indicates the tip of MC process. Note that MC extended a process along the Pecam1-EGFP-labeled inter-EC junctions.

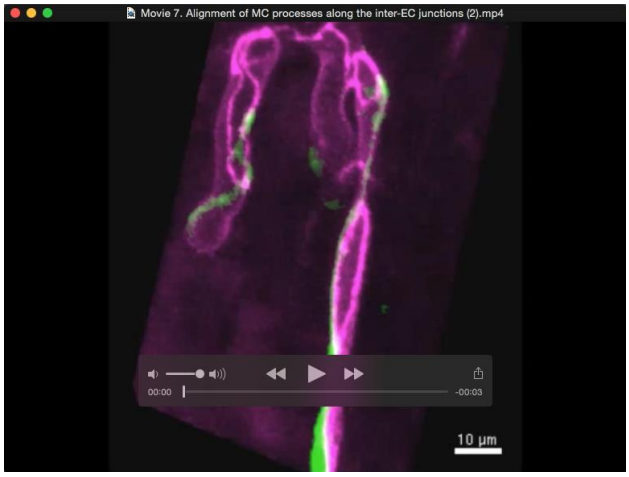

Movie 7. Alignment of MC processes along the inter-EC junctions.
3D-rotate image of CtA in the *TgBAC(pdgfrb:mCherry);Tg(fli1a:pecam1-EGFP)* larva at 4 dpf, as shown in Fig. **S3B**. Green, mCherry (MC); Magenta, EGFP (Pecam1-EGFP-labeled inter-EC junctions).

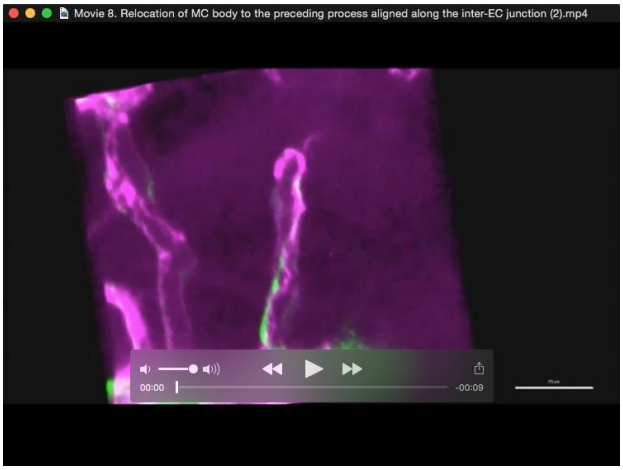

Movie 8. Relocation of MC body to the preceding process aligned along the inter-EC junction.

Time-lapse confocal imaging of CtA in the *TgBAC(pdgfrb:mCherry);Tg(fli1a:pecam1-EGFP)* larva starting from 62 hpf, as shown in Fig. **3C**. Images were obtained every 20 min. Green, mCherry (MC); magenta, EGFP (Pecam1-EGFP-labeled inter-EC junctions).

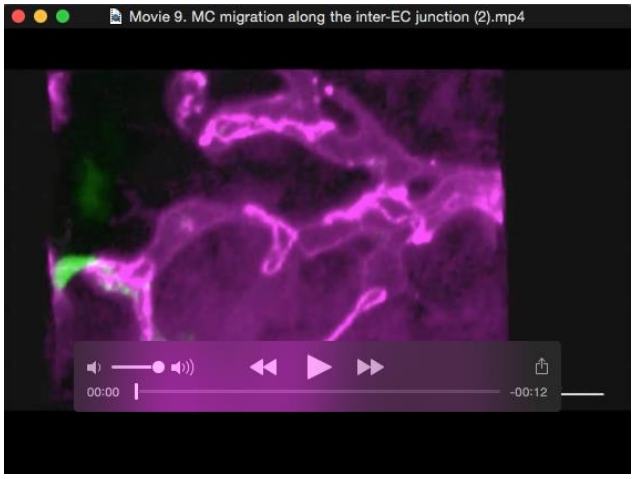

Movie 9. MC migration along the inter-EC junction.
Time-lapse confocal imaging of CtA in the *TgBAC(pdgfrb:mCherry);Tg(fli1a:pecam1-EGFP)* larva staring from 62 hpf, as shown in Fig. **S3C**. Images were obtained every 20 min. Green, mCherry (MC); magenta, EGFP (Pecam1-EGFP-labeled inter-EC junctions). The MC could extend its process across the unicellular EC tube without contacting with the inter-EC junctions. However, once the tip of the process reached to the inter-EC junction, the MC constantly extended its process along the junction and moved forward by relocating its cell body to the preceding process which aligned along the inter-EC junctions.

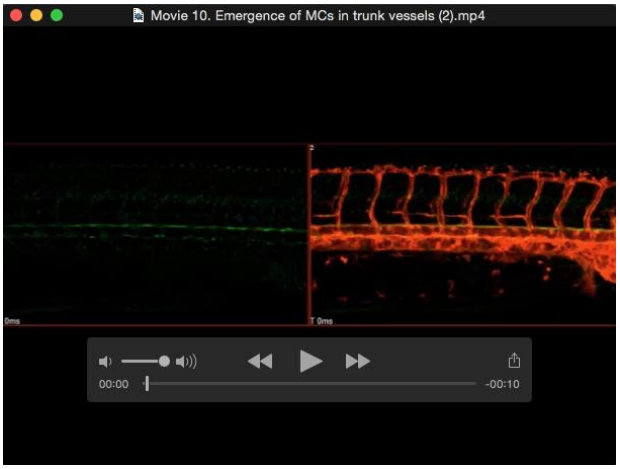

Movie 10. Emergence of MCs in trunk vessels.
Time-lapse confocal imaging of trunk vasculature in the *TgBAC(pdgfrb:EGFP);Tg(fli1a:Myr-mCherry)* embryo (46-76 hpf). Lateral view, anterior to the left. Left, EGFP image; right, merged image of EGFP (green) and mCherry (red).

Reference List

Asakawa,K., Suster,M.L., Mizusawa,K., Nagayoshi,S., Kotani,T., Urasaki,A., Kishimoto,Y., Hibi,M., and Kawakami,K. (2008). Genetic dissection of neural circuits by Tol2 transposon-mediated Gal4 gene and enhancer trapping in zebrafish. *Proc. Natl. Acad. Sci. U. S. A* 105, 1255-1260.

Distel,M., Wullimann,M.F., and Koster,R.W. (2009). Optimized Gal4 genetics for permanent gene expression mapping in zebrafish. *Proc. Natl. Acad. Sci. U. S. A* 106, 13365-13370.

Fukuhara,S., Zhang,J., Yuge,S., Ando,K., Wakayama,Y., Sakaue-Sawano,A., Miyawaki,A., and Mochizuki,N. (2014). Visualizing the cell-cycle progression of endothelial cells in zebrafish. *Dev. Biol.* 393, 10-23.

Her,G.M., Chiang,C.C., and Wu,J.L. (2004). Zebrafish intestinal fatty acid binding protein (I-FABP) gene promoter drives gut-specific expression in stable transgenic fish. *Genesis.* 38, 26-31.

Kawakami,K., Takeda,H., Kawakami,N., Kobayashi,M., Matsuda,N., and Mishina,M. (2004). A transposon-mediated gene trap approach identifies developmentally regulated genes in zebrafish. *Dev. Cell* 7, 133-144.

Kawamura,A., Koshida,S., Hijikata,H., Ohbayashi,A., Kondoh,H., and Takada,S. (2005). Groucho-associated transcriptional repressor ripply1 is required for proper transition from the presomitic mesoderm to somites. *Dev. Cell* 9, 735-744.

Kogata,N., Arai,Y., Pearson,J.T., Hashimoto,K., Hidaka,K., Koyama,T., Somekawa,S., Nakaoka,Y., Ogawa,M., Adams,R.H. et al. (2006). Cardiac ischemia activates vascular endothelial cadherin promoter in both preexisting vascular cells and bone marrow cells involved in neovascularization. *Circ. Res.* 98, 897-904.

Kwon,H.B., Fukuhara,S., Asakawa,K., Ando,K., Kashiwada,T., Kawakami,K., Hibi,M., Kwon,Y.G., Kim,K.W., Alitalo,K. et al. (2013). The parallel growth of motoneuron axons with the dorsal aorta depends on Vegfc/Vegfr3 signaling in zebrafish. *Development* 140, 4081-4090.

Lee,R.T., Knapik,E.W., Thiery,J.P., and Carney,T.J. (2013). An exclusively mesodermal origin of fin mesenchyme demonstrates that zebrafish trunk neural crest does not generate ectomesenchyme. *Development* 140, 2923-2932.

Reichenbach,B., Delalande,J.M., Kolmogorova,E., Prier,A., Nguyen,T., Smith,C.M., Holzschuh,J., and Shepherd,I.T. (2008). Endoderm-derived Sonic hedgehog and mesoderm Hand2 expression are required for enteric nervous system development in zebrafish. *Dev. Biol* 318, 52-64.

Rodrigues,F.S., Doughton,G., Yang,B., and Kelsh,R.N. (2012). A novel transgenic line using the Cre-lox system to allow permanent lineage-labeling of the zebrafish neural crest. *Genesis.* 50, 750-757.

Sehnert,A.J., Huq,A., Weinstein,B.M., Walker,C., Fishman,M., and Stainier,D.Y. (2002). Cardiac troponin T is essential in sarcomere assembly and cardiac contractility. *Nat. Genet.* 31, 106-110.

Urasaki,A., Morvan,G., and Kawakami,K. (2006). Functional dissection of the Tol2 transposable element identified the minimal cis-sequence and a highly repetitive sequence in the subterminal region essential for transposition. *Genetics* 174, 639-649.

Whitesell,T.R., Kennedy,R.M., Carter,A.D., Rollins,E.L., Georgijevic,S., Santoro,M.M., and Childs,S.J. (2014). An alpha-smooth muscle actin (acta2/alphasma) zebrafish transgenic line marking vascular mural cells and visceral smooth muscle cells. *PLoS. One.* 9, e90590.

Yusufzai,T.M. and Felsenfeld,G. (2004). The 5'-HS4 chicken beta-globin insulator is a CTCF-dependent nuclear matrix-associated element. *Proc. Natl. Acad. Sci. U. S. A* 101, 8620-8624.